22. OXYGEN AND CARBON ISOTOPE RECORD FOR THE EARLY AND MIDDLE MIOCENE IN THE CENTRAL EQUATORIAL PACIFIC (LEG 85) AND PALEOCEANOGRAPHIC IMPLICATIONS[1]

Edith Vincent and John S. Killingley, Scripps Institution of Oceanography[2]

ABSTRACT

Oxygen and carbon isotope stratigraphies are given for the planktonic foraminifer *Globoquadrina venezuelana* (a deep-dwelling species) at three DSDP sites located along a north–south transect at approximately 133°W across the Pacific equatorial high-productivity zone. The records obtained at Sites 573 and 574 encompass the lower Miocene. At Site 575 the record includes the middle Miocene and extends into the lowermost lower Miocene. The time resolution of the planktonic foraminifer isotope record varies from 50,000 to 500,000 yr. The benthic foraminifer *Oridorsalis umbonatus* was analyzed for isotope composition at a few levels of Site 575. Isotope stratigraphies for all three sites are compared with carbonate, foraminifer preservation, and grain size records. We identified a number of chemostratigraphic signals that appear to be synchronous with previously recognized signals in the western equatorial Pacific and the tropical Indian Ocean, and thus provide useful tools for chronostratigraphic correlations. The sedimentary sequence at Site 573 is incomplete and condensed, whereas the sequences from Sites 574 and 575 together provide a complete lower Miocene record. The expanded nature of this record, which was recovered with minimum disturbance and provides excellent calcareous and siliceous biostratigraphic control, offers a unique opportunity to determine the precise timing of early Miocene events. Paleomagnetic data from the hydraulic piston cores at Site 575 for the first time allow late early Miocene paleoceanographic events to be tied directly to the paleomagnetic time scale.

The multiple-signal stratigraphies provide clues for paleoceanographic reconstruction during the period of preconditioning before the major middle Miocene cooling. In the lowermost lower Miocene there is a pronounced shift toward greater $\delta^{13}C$ values (by $\sim 1‰$) within magnetic Chron 16 (between approximately 17.5 and 16.5 Ma). The "Chron 16 Carbon Shift" coincides with the cessation of an early Miocene warming trend visible in the $\delta^{18}O$ signals. Values of $\delta^{13}C$ remain high until approximately 15 Ma, then decrease toward initial (early Miocene) values near 13.5 Ma. The broad lower to middle Miocene $\delta^{13}C$ maximum appears to correlate with the deposition of organic-carbon-rich sediments around the margin of the northern Pacific in the Monterey Formation of California and its lateral equivalents. The sediments rimming the Pacific were probably deposited under coastal upwelling conditions that may have resulted from the development of a strong permanent thermocline. Deposition in the upwelling areas occurred partly under anaerobic conditions, which led to the excess extraction of organic carbon from the ocean. The timing of the middle Miocene cooling, which began after the Chron 16 Carbon Shift, suggests that the extraction of organic carbon preconditioned the ocean–atmosphere system for subsequent cooling.

A major carbonate dissolution event in the late early Miocene, starting at approximately 18.7 Ma, is associated with the enrichment in ^{13}C. The maximum dissolution is coeval with the Chron 16 Carbon Shift. It corresponds to a prominent acoustic horizon that can be traced throughout the equatorial Pacific.

INTRODUCTION

Among Cenozoic paleoceanographic events, the middle Miocene oxygen isotope step is of prime importance, because it probably marks the onset of modern ocean conditions, that is, ocean basins filled with water masses generated at high latitudes. The step consists of a sharp ^{18}O enrichment in benthic foraminifers representing a shift of about $+1‰$. This shift has been interpreted as reflecting a major buildup of Antarctic ice and a drop in surface-water temperatures on the Antarctic coast (Savin et al., 1975; Shackleton and Kennett, 1975; Woodruff et al., 1981). The concept of ice buildup at this time has been widely accepted, although there is disagreement about the amount of ice that was present before the middle Miocene (Matthews and Poore, 1980; Keigwin and Keller, 1984; Miller and Thomas, this volume). The cause of the proposed rapid increase in volume of the Antarctic ice sheet remains unknown; its explanation is a prime challenge of Cenozoic paleoceanography. Berger et al. (1981) pointed out that the rapidity of the glaciation suggests positive feedback within the system, presumably tied to albedo effects or to the CO_2 budget (Berger, 1982). Blanc et al. (1980), Schnitker (1980a, b), and Berggren and Schnitker (1983) have suggested that the Antarctic glaciation was triggered by a fundamental rearrangement of the North Atlantic circulation system that occurred when the Iceland Ridge subsided below a critical depth, an event that linked the entire north polar sea as a heat sink to the world ocean. More recently, Vincent et al. (1983) and Vincent and Berger (1984) have suggested that the extraction of organic carbon at the ocean margins in the latest early Miocene preconditioned the ocean–atmosphere for subsequent middle Miocene cooling. These authors suggest that the buildup of organic-carbon-rich sediments around the edge of the northern Pacific reduced the CO_2 concentration in the atmosphere and thus fostered the subsequent growth of ice in Antarctica.

The reconstruction of environmental conditions during the period before the middle Miocene cooling is crucial to an understanding of this event. To date, however,

[1] Mayer, L., Theyer, F., et al., *Init. Repts. DSDP*, 85: Washington (U.S. Govt. Printing Office).

[2] Addresses: (Vincent, present address) Département de Géologie Dynamique, Université Pierre et Marie Curie, 4 Place Jussieu, 75230 Paris Cedex 05, France; (Killingley) Scripps Institution of Oceanography, University of California at San Diego, La Jolla, CA 92093.

paleoceanographic studies of the early Miocene have been hampered by the paucity of complete and undisturbed sedimentary sequences. The recovery of expanded lower Miocene sections, with minimum disturbance and excellent calcareous and siliceous biostratigraphic control, during DSDP Leg 85 in the central equatorial Pacific offers a unique opportunity to investigate the environmental conditions prevailing during the early Miocene. The sequence at Site 575, which was recovered by hydraulic piston coring, is of special interest. Paleomagnetic data for the uppermost lower Miocene at this site permit for the first time biostratigraphic and paleoceanographic events to be tied directly to the paleomagnetic time scale.

MATERIAL OF STUDY

The sediments analyzed in this study were recovered at Sites 573, 574, and 575 in the central equatorial Pacific during DSDP Leg 85. These three sites are located along a north–south transect across the equatorial high-productivity zone along approximately 133°W. They lie at water depths ranging from 4300 to 4555 m near the crest of the equatorial sediment bulge (Table 1; Fig. 1). The three sites have migrated from south of the equator to deeper, more western locations at or north of the equator. The changes in productivity that accompanied the equatorial crossings (which occurred for the different sites at different times during the Miocene) are reflected in the sediments in changes in accumulation rates, siliceous microfossil abundance, and foraminiferal preservation. The basic patterns of Pacific equatorial sedimentation have been outlined by Berger and Winterer (1974), and models relating sedimentation and equatorial crossing have been elaborated by various authors (Winterer, 1973; van Andel et al., 1975; Lancelot, 1978). Sites 574 and 575 crossed the equator during the early Miocene, Site 573 during the late Miocene (Weinreich and Theyer, this volume). Previous DSDP holes drilled in this area include Sites 71 and 77, which provided valuable sections for Miocene paleoceanographic studies.

Lower Miocene sequences were recovered at Sites 573 and 574 by rotary coring. Disturbance was minor because of the induration of the sediments. The sequences are ~75 and 160 m thick, respectively, and they overlie Oligocene sediments. At Site 575, a 120-m-thick lower Miocene sequence was recovered by hydraulic piston corer (HPC); the section ended in lowermost lower Miocene sediments assigned an age of approximately 22 Ma. We recovered the stable isotope stratigraphies for the lower Miocene at these three sites. Other studies in this volume provide stable isotope stratigraphies for Site 574 for Oligocene (Miller and Thomas, this volume) and middle Miocene (Pisias et al., this volume) sediments. Our sampling ranges from the uppermost Oligocene to the lowermost middle Miocene at Sites 573 and 574. At Site 575 it encompasses the middle Miocene and was extended into the upper Miocene to obtain a continuous isotope record for the early to middle Miocene time interval.

Table 1A. Site locations.

Site	Location	Longitude	Water depth (m)
573	00°29.91′N	133°18.57′W	4.301
574	04°12.52′N	133°19.81′W	4.561
575	05°51.00′N	135°02.16′W	4.536

Table 1B. Material studied.

Hole	Cores	Coring method
573B	11 to 23	Rotary
574	25 to 31	HPC
574C	1 to 21	Rotary
575A	1 to 33	HPC
575B	2 to 14	HPC

The sediments consist of calcareous ooze and chalk with a high calcium carbonate content of 80 to 96% throughout most of the lower and middle Miocene. An interval with decreased calcium carbonate content occurs at all three sites in the uppermost lower Miocene with pronounced minima as low as 40 to 60% (Figs. 2 to 4). This interval of decreased $CaCO_3$ content (in the middle of the *Denticulopsis nicobarica* Zone, near 17 Ma) appears to correspond to a prominent and laterally traceable acoustic horizon (Mayer et al., this volume). At Site 575, centimeter-thick sandy turbidite layers containing mostly sand-sized foraminifers and volcanic debris are intercalated throughout the section. These layers were carefully skipped during sampling.

The abundance of both calcareous and siliceous microfossils throughout the sequences permits a multiple biostratigraphic zonation (Figs. 2 to 4). The ages indicated in Figures 2 to 4 are derived from diatom zonal boundaries and the time scale given by Barron et al. (this volume) and Barron et al. (in press), which is based on the paleomagnetic time scale of Berggren et al. (in press). Paleomagnetic data obtained from the upper lower Miocene in Hole 575A (Weinreich and Theyer, this volume) allow the identification of magnetic Anomalies 5C and 5D (Fig. 4). Biostratigraphic datums and paleoceanographic events of the late early Miocene can thus be directly tied for the first time to the magnetostratigraphy encompassing the middle of Chron 17 to the middle of Chron 16.

The average accumulation rate for the entire lower Miocene is approximately 9.7 m/m.y. at Site 573, 20.8 m/m.y. at Site 574, and 20 m/m.y. at Site 575. Middle Miocene sediments accumulated at Site 575 at an average rate of about 9 m/m.y., upper Miocene sediments at an average reduced rate of about 4.7 m/m.y. Our sampling interval, which is 1 m, thus corresponds to a time interval of roughly 103,000, 48,000, and 50,000 yr. for the lower Miocene at Sites 573, 574, and 575, respectively. For the middle Miocene at Site 575 it corresponds to 110,000 yr. and for the upper Miocene, to 212,000 yr. (Barron et al., this volume).

All samples (20 cm^3) were dried, weighed, soaked in buffered Calgon solution, washed on a 63-μm sieve, and cleaned ultrasonically to remove fine particles from inside the foraminifer test. Residues were then dried and weighed. Results of grain size analyses are listed in Table 2 and plotted in Figures 2 to 4. Calcium carbonate con-

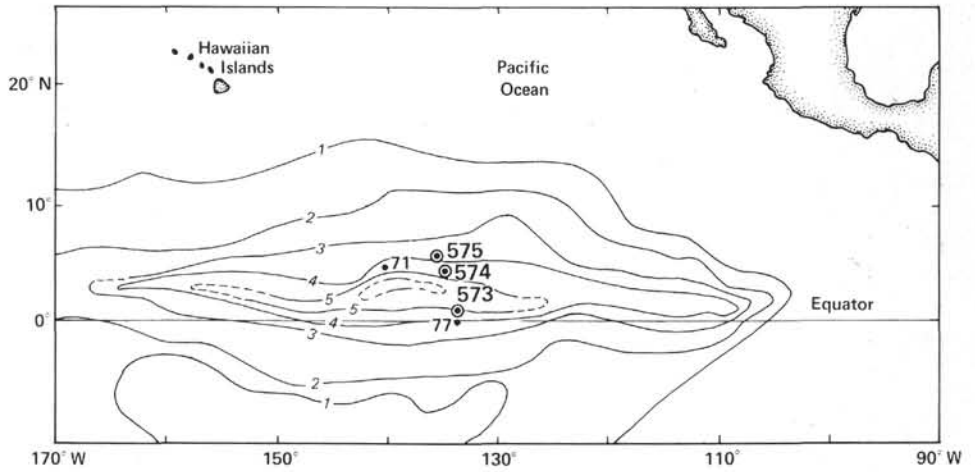

Figure 1. Location of DSDP Sites 573, 574, and 575 (⊙) and of previous DSDP Sites 71 and 77 (●) in the central equatorial Pacific in relationship to sediment thickness (contours in tenths of seconds of two-way traveltime).

tents obtained from shipboard carbonate bomb analyses at 1.5-m intervals (see site chapters, this volume) are plotted in Figures 2 to 4. Because of time constraints, not all samples were analyzed for isotope composition. Approximately 200 samples were analyzed for both oxygen and carbon isotopes by following our standard procedure (Berger and Killingley, 1977). The time resolution of our isotope stratigraphies is roughly 500,000, 170,000, and 50,000 yr. for the early Miocene at Sites 573, 574, and 575, respectively. For the middle Miocene at Site 575 it is roughly 280,000 yr., and for the late Miocene it is 700,000 yr.

Foraminifers are abundant throughout the sequences; preservation is good to moderate. Fluctuations in the preservation of planktonic foraminifers are indicated by the foraminifer preservation curves constructed by Saito (this volume) from core-catcher samples using the codes of Berger and von Rad (1972) (Figs. 2 to 4). Throughout the lower Miocene, preservation is better at Site 575 than at Sites 573 and 574, probably because of the earlier equatorial crossing of Site 575 during the early Miocene. At all three sites there is an interval with poorer foraminifer preservation in the uppermost lower Miocene in the N6–N8 zonal interval, which corresponds to the interval of decreased $CaCO_3$ content. The elimination of solution-susceptible species in this interval precludes the identification of Zone N7.

We established continuous isotope stratigraphies for the deep-dwelling planktonic foraminifer *Globoquadrina venezuelana*. To minimize the effect of ontogenetic development on the isotope composition of the test (Berger et al., 1978), specimens were selected from a restricted size range (350 to 420 μm). We chose *G. venezuelana* because this species is common throughout the sequences. Furthermore, our various studies have shown this species to be the most reliable deep-dwelling planktonic foraminifer for Neogene reconstruction (Vincent et al., 1980; in press). We can thus compare our results with isotope stratigraphies obtained from the same species in the Miocene of the tropical Indian Ocean (Vincent et al., in press), where we also obtained an isotope record from shallow-dwelling planktonic and benthic foraminifers. Because of the time constraints of this study, benthic foraminifers (*Oridorsalis umbonatus*) were analyzed at only a few levels of Site 575.

RESULTS

Isotope Stratigraphy

Isotope values of *Globoquadrina venezuelana* are given in Table 3 and are plotted versus depth and biostratigraphic zonation in Figures 2 to 4. Despite the problems that occurred as the result of varying sampling density, general trends could be identified and isotope events could be correlated between sites. The isotope curves reveal a succession of stratigraphic intervals with distinct isotopic signatures. The levels marking the boundaries between these intervals have been labeled in a stratigraphic order from bottom to top with capital letters (A to H). Their biostratigraphic position is given in Figure 5.

Oxygen Isotope Stratigraphy

Throughout the uppermost Oligocene and the lower half of the lower Miocene, up to level C, there is no definite trend in the oxygen isotope record of *Globoquadrina venezuelana*. The $\delta^{18}O$ values range between 0.5 and 1.5‰, with rather large fluctuations (up to 0.8‰). From level C to level F, throughout the upper half of the lower Miocene, there is a regular and steady decrease in the $\delta^{18}O$ values from approximately 1‰ to 0‰. Variations in this interval are of low amplitude. At level F, in the uppermost lower Miocene, the $\delta^{18}O$ values are the lowest of the entire record (−0.2‰). Immediately above this level, there is an abrupt enrichment in ^{18}O of over 1‰ within 2 m.

Above this offset, the isotope stratigraphy can be followed at Site 575 only. In the interval between levels F and G, which spans the lower/middle Miocene boundary, $\delta^{18}O$ values decrease slightly, with a mean of about 0.8‰. In the lower half of this interval, there is little variability at Site 575, in contrast to results from Site 574, where large-amplitude fluctuations occur. In the next

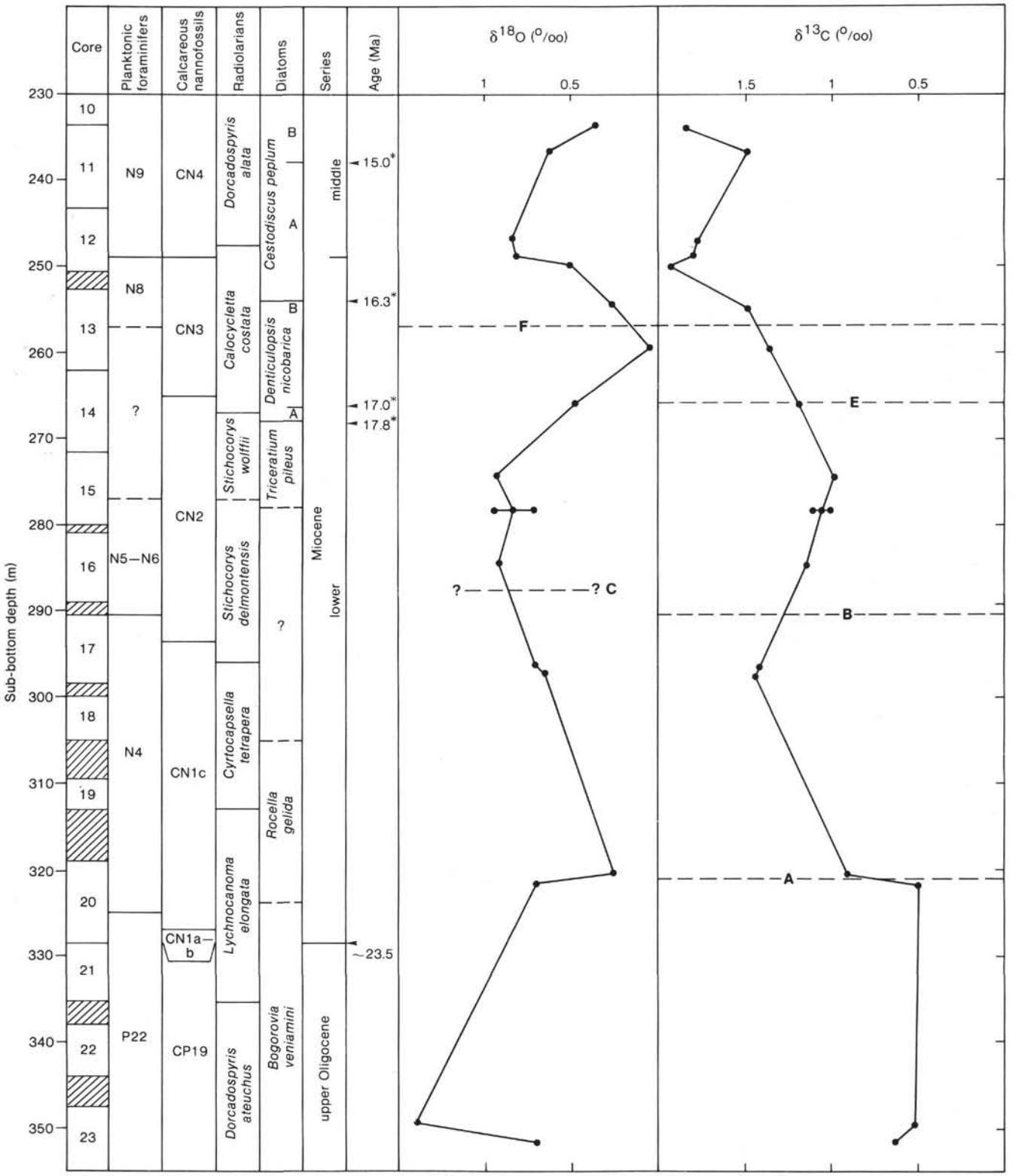

Figure 2. Biostratigraphy and changes at Site 573 in stable isotope composition of the deep-dwelling planktonic foraminifer *Globoquadrina venezuelana*, in sand fraction (>63 μm) content, in $CaCO_3$ content, and in foraminiferal solution (FS). Biostratigraphy at left is a composition column established from the various holes at this site by Saito (this volume) for foraminifers, Pujos (this volume) for calcareous nannofossils, Nigrini (this volume) for radiolarians, and Barron (this volume) for diatoms. Except for the earliest age at the Oligocene/Miocene boundary, ages are from diatom zonal boundaries according to Barron (this volume) and Barron et al. (in press). Asterisks indicate those derived from direct paleomagnetic calibration. Oxygen and carbon isotope data are from Table 3 and those for sand fraction content from Table 2. Calcium carbonate data are from shipboard analyses (site chapters, this volume). Foraminiferal solution data are from Saito (site chapters, this volume) following the codes of Berger and von Rad (1972). Increasing values indicate more pronounced dissolution. Stratigraphic levels A to G are defined in Figure 5.

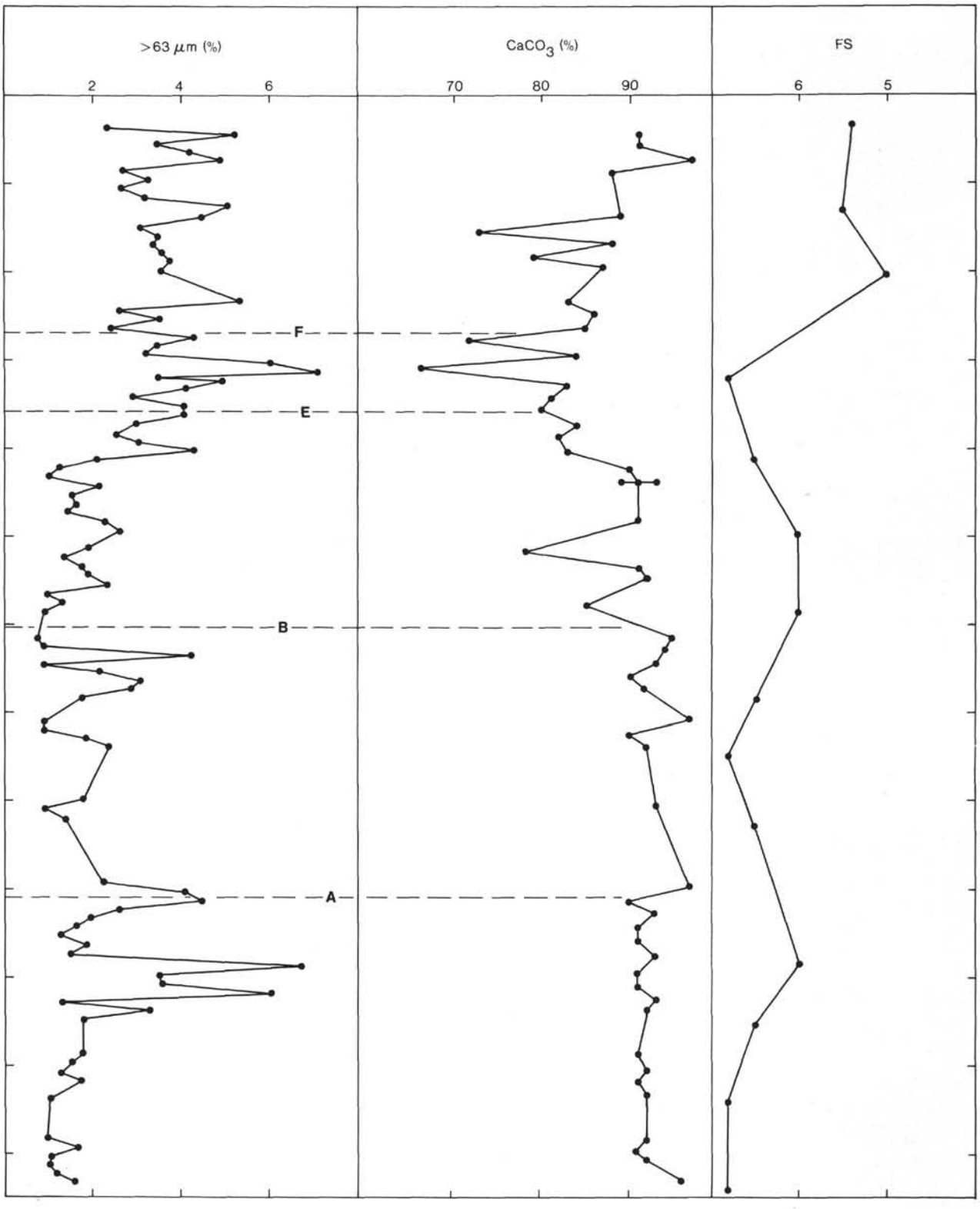

Figure 2. (Continued).

interval, from levels G to H in the middle Miocene, $\delta^{18}O$ values show high-amplitude, high-frequency fluctuations, with an overall increase in $\delta^{18}O$ of approximately 0.7‰. Above level H, $\delta^{18}O$ values show a significant decrease of about 1‰ throughout the remainder of the middle Miocene to values near 0.7‰. In the upper Miocene $\delta^{18}O$ remains close to this value. The upper Miocene sequence at Site 575 is condensed and incomplete and is not well suited to detailed stratigraphy (note the low carbonate values).

A detailed comparison between the planktonic and benthic foraminifer isotope records at Site 575 cannot

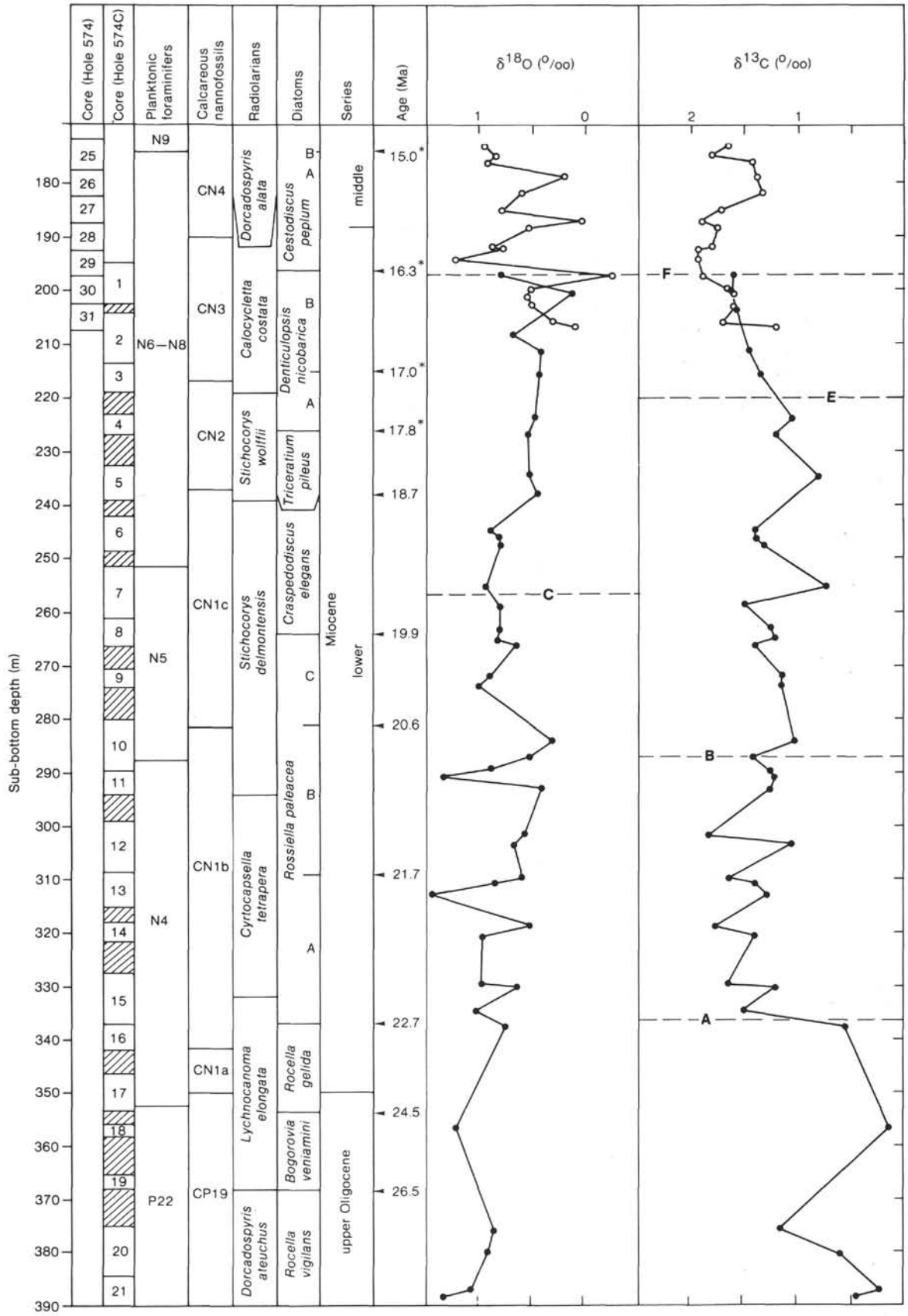

Figure 3. Biostratigraphy and changes at Site 574 in stable isotope composition of *Globoquadrina venezuelana*, in sand fraction content, in $CaCO_3$ content, and in foraminiferal solution (FS). See Figure 2 legend for data origin and other details. Solid black dots indicate data from Hole 574C, open dots data from Hole 574.

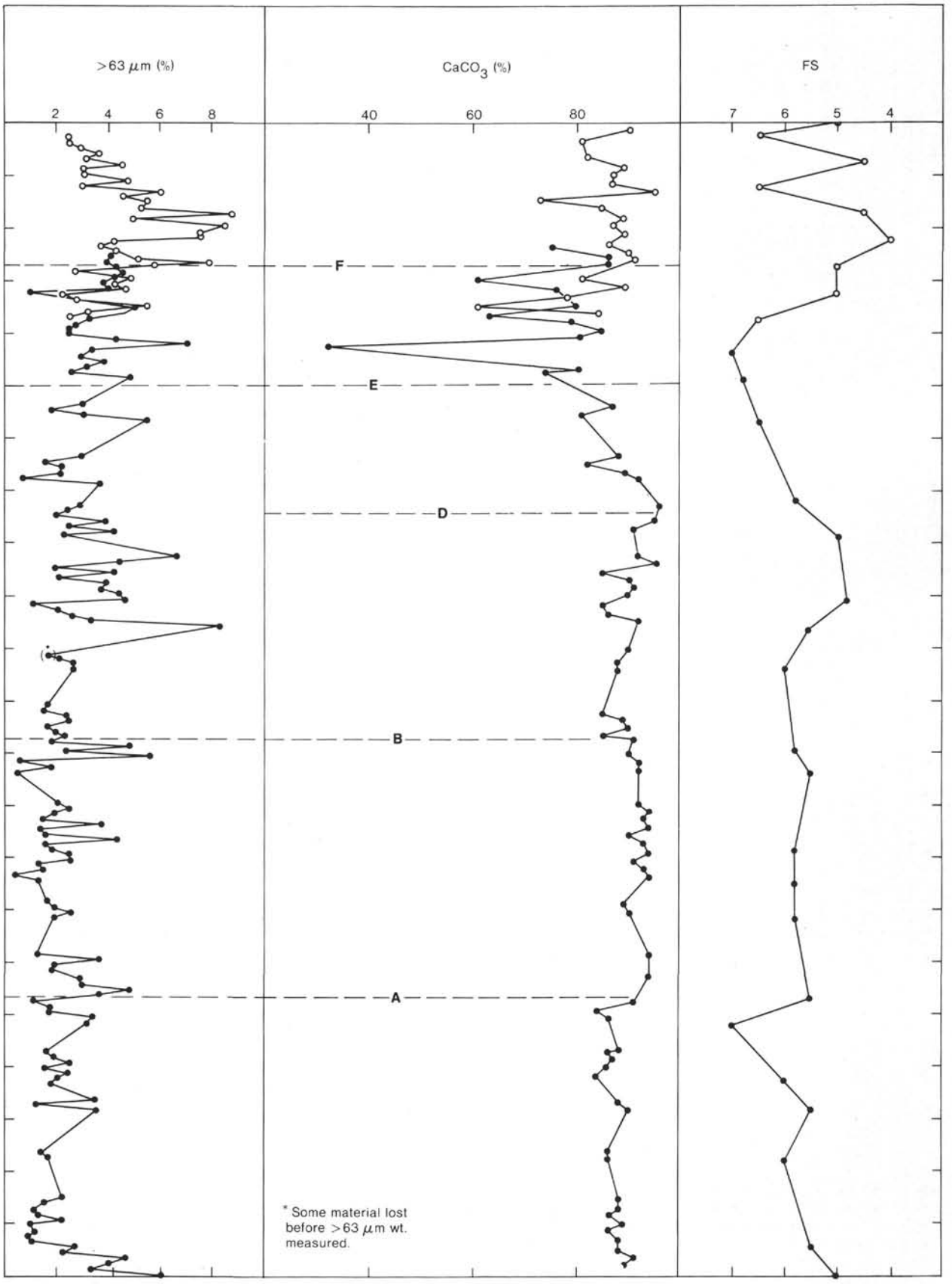

Figure 3. (Continued).

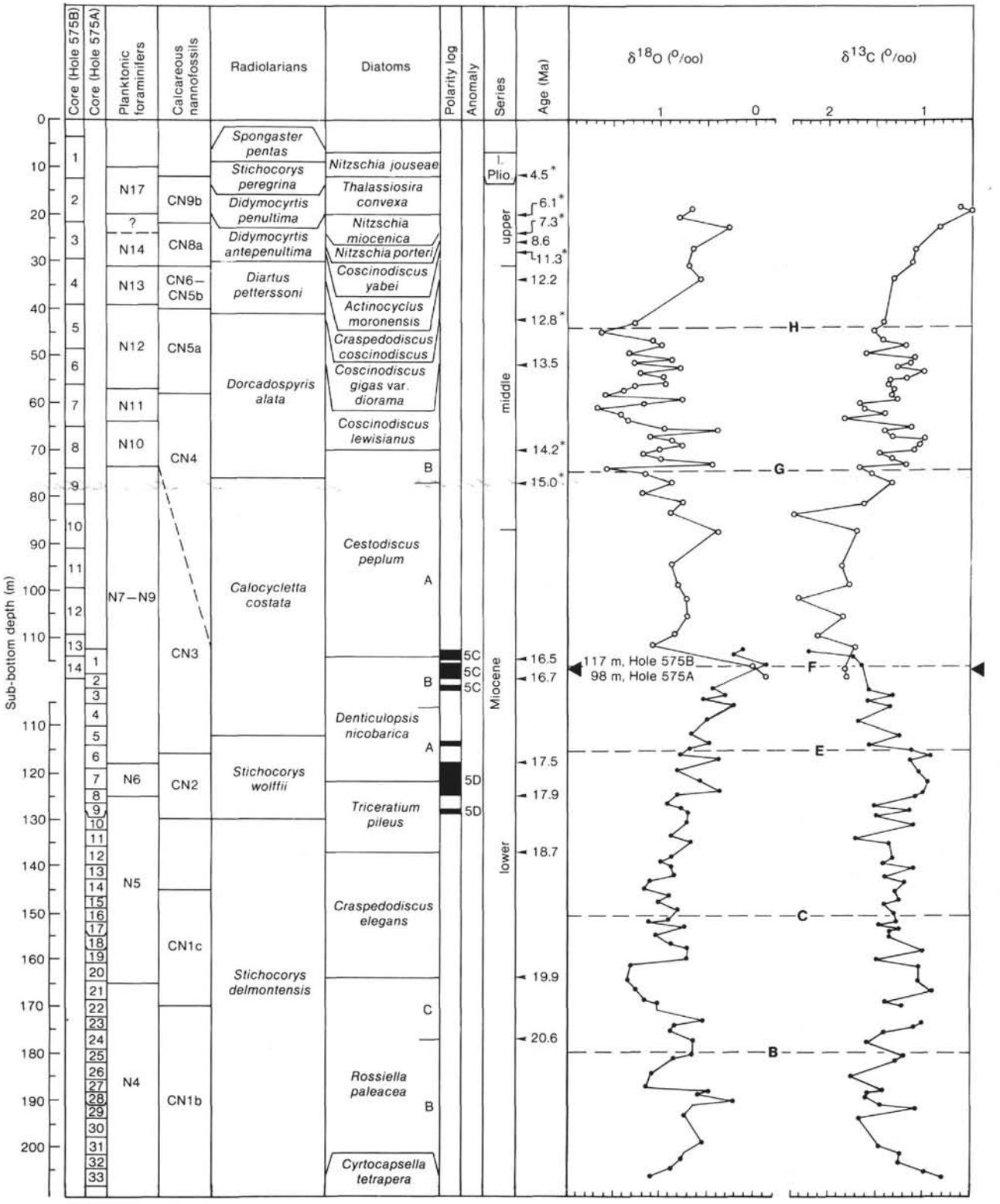

Figure 4. Biostratigraphy, magnetostratigraphy, and changes at Site 575 in stable isotope composition of *Globoquadrina venezuelana*, in sand fraction content, in $CaCO_3$ content, and in foraminiferal solution (FS). See Figure 2 legend for data origin and other details. The magnetic polarity log in the interval between Cores 575A-1 and 575A-10 is from Weinreich and Theyer (this volume). Ages given in this interval are derived from the boundaries between revised and normal intervals. Solid black dots indicate data from Hole 575A, open dots data from Hole 575B. There is a 19-m offset in the sub-bottom depths given for the cores of Hole 575A as compared with Hole 575B. To obtain the real sub-bottom depths of these cores, a value of 19 m should be added to the nominal depths indicated at the left of Hole 575A. A correlation point between Holes 575A and 575B is obtained by a turbidite horizon in Core 575B-14 (117 m sub-bottom) and Core 575A-1 (98 m nominal sub-bottom). This horizon is indicated with a solid triangle. This correlation between the two holes is in good agreement with the isotope, sand content, and carbonate data within the interval of overlap and with biostratigraphic data given in the site chapters (this volume).

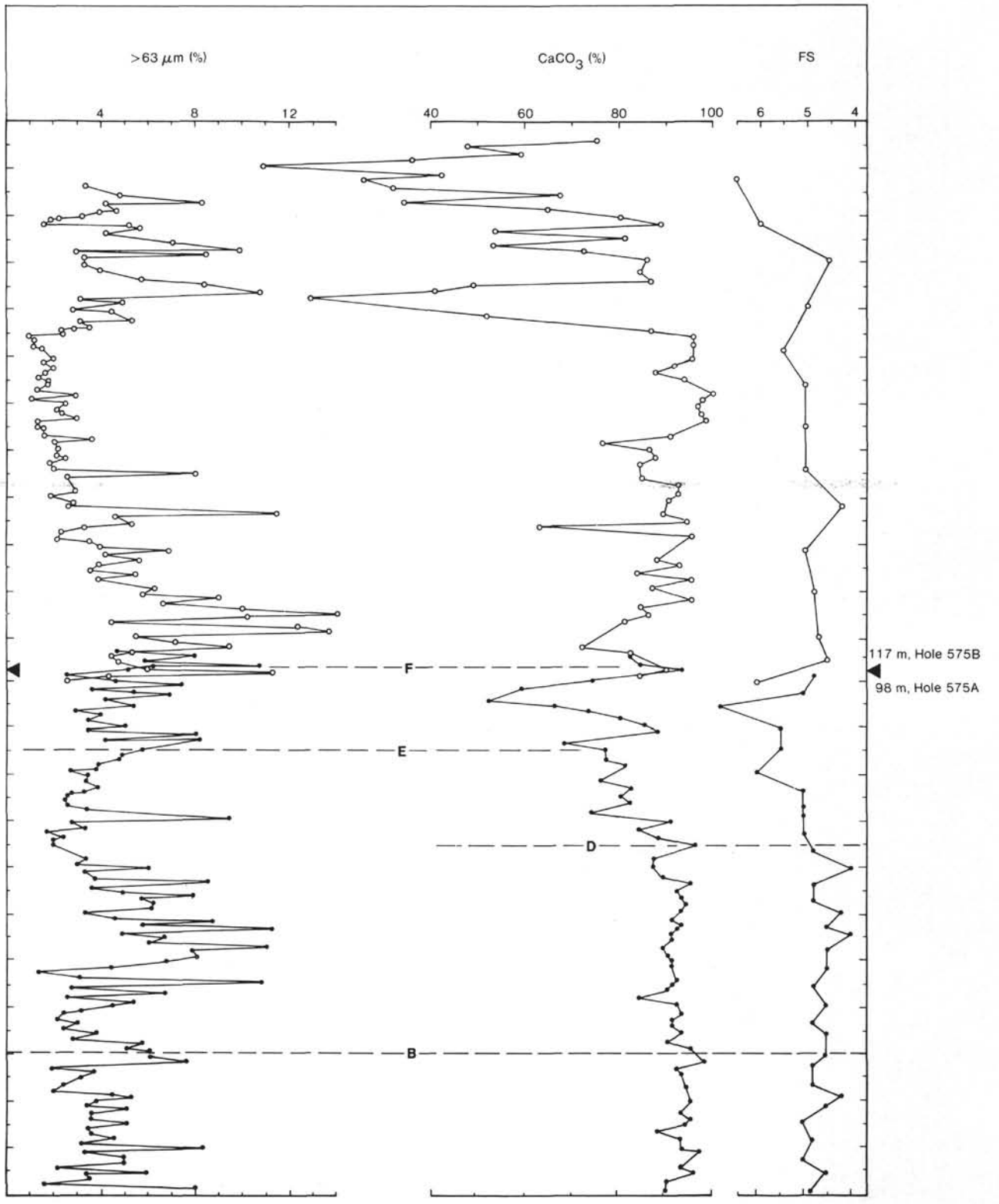

Figure 4. (Continued).

be made because of the wide spacing between the benthic data (Table 4; Fig. 6). However, a few features are apparent. The $\delta^{18}O$ values of *Oridorsalis umbonatus* show a slight upwardly decreasing trend in the lower Miocene interval between levels C and E. The trend parallels the decreasing trend of *G. venezuelana*. In the interval between levels F and G, which spans the lower/middle Miocene boundary, the benthic foraminifers have a constant $\delta^{18}O$ value of 2‰. At level G in the middle Miocene the signature of the *G. venezuelana* record changes

Table 2. Percentages of the sand fraction (>63 μm) in sediments of Holes 573B, 574, 574C, 575A, and 575B.

Core-Section (interval in cm)	Sub-bottom depth (m)	>63 μm (%)
Hole 573B		
11-1, 6-10	233.58	2.4
1, 103-107	234.55	5.1
2, 50-54	235.52	3.5
3, 7-11	236.59	4.2
3, 98-102	237.50	4.9
4, 50-54	238.52	2.6
5, 5-9	239.57	3.3
5, 101-105	240.53	2.6
6, 49-53	241.51	3.2
7, 5-9	242.57	5.1
12-1, 92-96	243.94	4.4
2, 46-50	244.98	3.0
2, 146-150	245.98	3.5
3, 98-102	247.00	3.4
4, 50-54	248.02	3.6
4, 146-150	248.98	3.7
5, 98-102	250.00	3.5
13-1, 80-84	253.32	5.3
2, 28-32	254.30	2.6
2, 130-134	255.32	3.6
3, 80-84	256.32	2.4
4, 32-36	257.34	4.3
4, 133-137	258.35	3.4
5, 78-80	259.29	3.1
6, 30-34	260.32	6.0
6, 130-134	261.32	7.1
7, 46-50	261.98	3.5
14-1, 28-30	262.29	5.0
1, 129-133	263.31	4.1
2, 75-79	264.27	2.9
3, 21-25	265.23	4.1
3, 120-124	266.22	4.1
4, 78-82	267.30	2.9
5, 28-32	268.30	2.5
5, 127-131	269.29	3.1
6, 73-77	270.25	4.3
7, 26-30	271.28	2.1
15-1, 64-68	272.16	1.3
2, 17-21	273.19	1.0
2, 118-122	274.20	2.2
3, 65-69	275.17	1.5
4, 18-22	276.20	1.7
4, 119-123	277.21	1.5
5, 71-75	278.23	2.3
6, 25-29	279.27	2.6
16-1, 38-42	281.40	1.9
1, 138-140	282.39	1.3
2, 86-90	283.38	1.7
3, 36-40	284.38	1.9
3, 145-149	285.47	2.4
4, 95-99	286.47	1.0
5, 49-53	287.51	1.4
6, 6-10	288.58	0.9
17-1, 95-99	291.47	0.8
2, 50-54	292.52	0.9
3, 3-7	293.55	4.1
3, 101-105	294.53	0.9
4, 50-54	295.52	2.2
4, 146-150	296.48	3.1
5, 82-86	297.34	2.9
6, 15-19	298.17	1.8
18-1, 100-104	301.02	0.9
2, 45-49	301.97	0.9
2, 146-150	302.98	1.9
3, 98-102	304.00	2.4
19-1, 48-52	310.00	1.8
1, 144-148	310.96	0.9
2, 100-104	312.02	1.4
20-1, 16-20	319.18	2.3
1, 119-123	320.21	4.1
2, 74-78	321.26	4.5
3, 20-24	322.22	2.5
3, 121-125	323.23	1.9

Table 2. (Continued).

Core-Section (interval in cm)	Sub-bottom depth (m)	>63 μm (%)
Hole 573B (Cont.)		
4, 68-72	324.20	1.7
5, 27-31	325.29	1.3
5, 130-134	326.32	1.9
6, 80-84	327.32	1.5
21-1, 18-22	328.70	6.8
1, 120-124	329.72	3.5
2, 75-79	330.77	3.6
3, 28-32	331.80	6.0
3, 136-140	332.88	1.3
4, 88-92	333.90	3.3
5, 30-34	334.82	1.8
22-1, 80-84	338.82	1.8
2, 31-35	339.83	1.5
2, 130-134	340.82	1.3
3, 76-80	341.78	1.7
4, 30-34	342.82	2.8
4, 129-133	343.81	1.0
23-1, 80-84	347.50	0.9
2, 36-40	349.38	1.7
2, 134-138	350.36	1.1
3, 90-94	351.42	1.0
4, 30-34	352.32	1.2
4, 130-134	353.32	1.6
Hole 574		
25-1, 11-14	172.63	2.5
1, 114-117	173.66	2.5
2, 64-69	174.67	2.9
3, 14-19	175.67	3.6
3, 124-128	176.76	3.2
26-1, 31-40	177.86	4.6
1, 130-137	178.84	3.0
2, 73-80	179.76	4.7
3, 32-39	180.86	3.1
3, 130-138	181.84	3.0
27-1, 65-72	182.89	6.1
2, 21-28	183.95	4.5
2, 123-129	184.96	5.5
3, 82-89	186.06	5.2
4, 22-29	186.96	8.8
28-1, 89-97	188.13	5.0
2, 41-47	189.14	8.5
3, 3-9	190.26	7.6
3, 92-99	191.16	7.6
4, 42-50	192.16	4.2
29-1, 100-107	193.24	3.6
2, 50-57	194.24	4.3
3, 2-9	195.26	5.2
3, 93-100	196.17	7.9
4, 33-40	197.07	5.8
30-1, 94-100	198.17	2.7
2, 51-58	199.25	4.8
3, 2-9	200.26	4.2
3, 102-107	201.25	4.6
31-1, 2-9	202.26	2.2
1, 101-109	203.25	2.8
2, 48-56	204.22	5.5
3, 2-8	205.25	3.2
3, 101-109	206.25	2.5
Hole 574C		
1-1, 75-79	195.27	4.1
2, 25-29	196.27	4.0
2, 125-129	197.27	4.2
3, 80-84	198.32	4.5
4, 30-34	199.32	4.2
4, 131-135	200.33	3.8
5, 80-84	201.32	4.0
6, 7-11	202.09	1.0
2-1, 100-104	205.02	5.0
2, 52-56	206.04	4.6

Table 2. (Continued).

Core-Section (interval in cm)	Sub-bottom depth (m)	>63 μm (%)
Hole 574C (Cont.)		
3, 2–6	207.04	3.2
3, 101–105	208.03	2.9
4, 53–57	209.05	2.5
5, 3–7	210.05	2.4
5, 101–105	211.03	4.2
6, 46–50	211.98	7.0
7, 2–6	213.04	3.3
3-1, 67–71	214.19	2.9
2, 15–19	215.17	3.8
2, 116–120	216.18	3.1
3, 68–72	217.20	2.6
4, 16–20	218.18	4.8
4-1, 34–38	223.36	2.9
1, 135–139	224.37	1.8
2, 83–87	225.35	3.0
3, 49–53	226.51	5.4
5-1, 100–104	233.52	2.9
2, 50–54	234.52	1.5
3, 2–6	235.54	2.2
3, 96–100	236.48	2.1
4, 52–56	237.54	0.6
5, 2–6	238.54	3.6
6-1, 80–84	242.82	2.9
2, 30–34	243.82	2.4
2, 131–135	244.83	1.9
3, 82–135	245.84	3.8
4, 30–34	246.82	2.4
4, 129–133	247.81	4.2
5, 30–34	248.32	2.2
7-1, 100–104	252.52	6.6
2, 52–56	253.54	4.4
3, 3–7	254.55	1.9
3, 102–106	255.54	4.2
4, 51–55	256.53	2.0
5, 2–6	257.54	3.9
5, 100–104	258.52	3.7
6, 51–55	259.53	4.3
7, 8–12	260.60	4.6
8-1, 53–57	261.55	1.1
2, 2–6	262.54	2.1
2, 100–104	263.52	2.5
3, 51–55	264.53	3.3
4, 3–7	265.55	7.3
9-1, 68–72	271.20	1.6
2, 26–30	272.28	2.0
2, 125–129	273.27	2.6
3, 72–76	274.24	2.6
10-1, 80–84	280.82	1.6
2, 28–32	281.80	1.4
2, 130–134	282.82	2.3
3, 80–84	283.82	2.4
4, 30–34	284.82	1.6
4, 131–135	285.83	1.9
5, 74–79	286.76	2.2
6, 26–30	287.78	1.7
6, 125–129	288.77	4.7
7, 43–47	289.45	2.3
11-1, 96–100	290.48	5.6
2, 51–55	291.53	0.5
3, 3–7	292.55	1.7
3, 101–105	293.53	0.5
12-1, 52–56	299.54	2.0
2, 2–6	300.54	2.4
2, 105–109	301.57	1.8
3, 55–59	302.57	1.4
3, 146–150	303.48	3.7
4, 94–98	304.46	1.2
5, 50–54	305.52	1.5
6, 3–7	306.55	4.3
6, 101–105	307.53	1.5
7, 30–34	308.32	1.7
13-1, 94–98	309.46	2.4
2, 31–35	310.33	2.5
2, 135–139	311.37	1.2
3, 90–94	312.42	1.4

Table 2. (Continued).

Core-Section (interval in cm)	Sub-bottom depth (m)	>63 μm (%)
Hole 574C (Cont.)		
4, 36–40	313.38	0.3
4, 131–135	314.33	1.2
14-1, 35–39	318.37	1.6
1, 136–140	319.38	1.8
2, 78–82	320.30	2.4
3, 30–34	321.32	1.8
15-1, 100–104	328.52	1.2
2, 37–41	329.39	3.5
2, 138–142	330.40	1.8
3, 80–84	331.32	1.8
4, 26–30	332.28	2.4
4, 129–133	333.31	2.8
5, 81–85	334.33	2.9
6, 29–33	335.31	4.8
6, 136–140	336.38	3.7
16-1, 55–59	337.57	1.1
2, 4–8	338.56	1.7
2, 103–107	339.55	1.6
3, 54–58	340.56	3.3
4, 32–36	341.84	3.1
17-1, 81–85	347.33	1.5
2, 32–36	348.34	1.8
2, 133–137	349.35	2.4
3, 76–80	350.28	1.5
4, 26–30	351.28	2.3
4, 131–135	352.33	2.0
5, 70–74	353.22	1.7
18-1, 25–74	356.27	3.4
1, 120–124	357.22	1.1
2, 74–78	358.26	3.5
19-1, 86–90	366.38	1.4
2, 33–37	367.35	1.5
20-1, 30–34	375.32	2.1
1, 125–129	376.27	1.4
2, 87–91	377.39	1.0
3, 44–48	378.46	1.1
4, 2–6	379.54	2.2
4, 100–104	380.52	1.0
5, 51–55	381.53	1.1
5, 146–150	382.48	0.8
6, 93–97	383.45	0.9
21-1, 30–34	384.82	2.6
1, 134–138	385.86	2.1
2, 80–84	386.82	4.6
3, 30–34	387.82	2.9
3, 131–135	388.83	3.3
4, 79–83	389.81	6.0
Hole 575A		
1-1, 2–9	93.85	4.7
1, 102–109	94.85	8.0
2, 61–68	95.94	5.9
3, 10–17	96.93	10.8
3, 134–141	98.18	6.2
4, 43–50	98.76	5.2
2-2, 31–38	99.05	2.6
2, 130–137	100.04	4.6
3, 81–88	101.05	7.5
4, 32–36	102.04	3.7
3-1, 130–137	102.43	5.4
2, 53–60	103.17	6.9
3, 10–19	104.24	4.2
4-1, 21–29	105.45	5.4
1, 122–128	106.45	3.0
2, 81–88	107.55	4.0
3, 45–52	108.69	3.5
4, 2–9	109.76	4.5
5-1, 142–149	110.46	3.5
2, 94–100	111.47	8.0
3, 52–59	112.56	4.3
4, 2–9	113.56	8.2
6-1, 61–68	114.74	5.8
2, 21–28	115.85	4.9
2, 121–128	116.85	4.4

Table 2. (Continued).

Core-Section (interval in cm)	Sub-bottom depth (m)	>63 μm (%)
Hole 575A (Cont.)		
3, 81–88	117.94	3.9
4, 41–48	119.05	3.8
7-1, 101–108	119.45	2.8
2, 52–59	120.46	3.5
2, 142–149	121.36	3.4
3, 130–138	122.74	3.9
8-1, 53–60	123.67	3.3
1, 102–109	124.15	2.9
8-2, 2–9	124.65	2.6
2, 102–109	125.65	2.5
9-1, 122–129	126.56	2.6
2, 81–88	127.64	3.4
10-1, 93–100	128.26	5.4
2, 49–56	129.33	9.5
3, 2–9	130.35	2.8
3, 104–111	131.38	3.3
11-2, 7–14	132.21	1.8
2, 102–109	133.15	2.4
3, 35–41	133.98	2.0
3, 131–138	134.94	2.0
12-1, 72–80	135.86	
2, 27–35	136.91	
2, 134–141	137.97	3.3
3, 94–101	139.07	3.0
13-1, 101–108	139.85	6.0
2, 50–57	140.84	2.7
3, 6–13	141.89	3.8
14-1, 111–118	143.05	8.6
2, 64–71	144.08	3.6
3, 13–20	145.07	5.0
3, 104–111	145.98	7.9
15-2, 25–31	146.48	5.8
2, 125–131	147.48	6.3
3, 89–97	148.63	6.2
16-2, 8–15	149.62	3.4
2, 104–111	150.58	4.6
3, 54–61	151.58	8.8
17-2, 53–60	152.07	5.9
3, 8–15	153.12	11.3
18-1, 128–135	153.82	5.0
2, 68–75	154.72	6.7
3, 28–35	155.82	6.0
3, 129–136	156.83	11.1
19-1, 89–86	157.72	8.0
2, 49–56	158.83	8.1
3, 2–9	159.85	6.8
20-1, 22–29	161.06	4.5
1, 128–135	162.12	1.4
2, 88–95	163.22	3.1
3, 49–56	164.33	10.9
21-1, 82–89	165.56	2.8
2, 30–37	166.54	6.8
2, 131–138	167.55	2.6
3, 81–88	168.55	5.4
22-1, 102–109	169.15	4.5
2, 44–52	170.08	3.2
2, 133–140	170.97	2.4
3, 92–99	172.06	2.2
23-1, 92–99	173.06	3.1
2, 51–58	174.14	2.5
24-1, 101–109	175.25	3.9
2, 52–59	176.26	2.8
3, 12–19	177.36	5.8
3, 102–109	178.26	5.1
4, 22–29	178.96	6.1
25-2, 143–150	180.17	6.1
3, 103–110	181.27	7.7
26-1, 132–139	181.46	2.7
2, 90–97	182.53	1.9
3, 31–38	183.44	2.7
3, 130–137	184.43	3.2
27-1, 130–137	186.24	2.4
2, 88–97	187.33	2.0
3, 30–37	188.24	4.5
28-1, 143–150	188.67	5.3

Table 2. (Continued).

Core-Section (interval in cm)	Sub-bottom depth (m)	>63 μm (%)
Hole 575A (Cont.)		
2, 100–107	189.74	3.8
3, 14–21	190.38	3.4
29-1, 141–148	191.15	5.1
2, 101–109	192.25	3.6
3, 52–59	193.26	3.6
30-1, 63–70	194.26	5.1
2, 23–30	195.36	3.5
2, 130–137	196.43	3.6
3, 90–97	197.53	4.7
31-1, 128–135	198.72	3.2
2, 65–72	199.59	8.3
3, 13–20	200.57	3.3
3, 101–108	201.45	5.0
32-1, 143–150	202.76	5.0
2, 92–100	203.76	2.2
3, 48–55	204.81	5.9
33-1, 92–99	205.26	3.4
2, 50–57	206.34	3.5
3, 2–9	207.35	1.6
3, 85–92	208.18	8.8
Hole 575B		
2-2, 67–71	14.19	5.4
3, 116–120	16.18	4.8
4, 86–90	17.38	8.2
5, 6–10	18.08	4.2
5, 117–121	19.19	4.6
6, 8–12	19.60	3.9
6, 107–111	20.59	3.2
7, 36–40	21.38	1.8
3-1, 123–127	22.25	1.6
1, 143–147	22.45	5.2
2, 45–49	22.97	5.4
3, 18–22	24.20	4.2
4, 54–58	26.06	7.0
5, 63–67	27.65	9.8
5, 103–107	28.05	3.0
5, 3–7	28.55	8.4
6, 101–105	29.53	3.3
4-1, 123–127	30.75	3.3
2, 76–80	31.78	2.9
3, 24–28	32.76	
3, 128–132	33.80	5.7
4, 80–84	34.82	8.4
5, 90–94	36.42	10.7
6, 120–124	38.22	3.1
7, 20–24	38.72	4.8
5-1, 128–132	40.30	2.8
2, 26–30	40.78	4.4
3, 13–17	42.15	5.2
3, 113–117	43.15	3.1
4, 3–7	43.55	3.2
4, 69–73	44.21	2.8
4, 144–148	44.96	2.3
5-5, 3–7	45.05	2.3
5, 103–107	46.05	1.0
6, 50–54	47.02	1.1
7, 3–7	48.05	1.1
6-1, [illegible]–69	48.67	1.5
2, 24–28	49.76	1.6
2, 123–127	50.75	1.9
3, 69–73	51.71	1.6
4, 25–29	52.77	1.9
4, 124–128	53.76	1.6
5, 85–89	54.87	1.4
6, 32–36	55.84	1.7
-1, 93–97	56.35	1.6
2, 47–51	57–39	1.3
3, 3–7	58.45	2.8
3, 95–99	59.37	1.1
4, 50–54	60.42	2.4
5, 3–7	61.45	2.1
5, 105–109	62.47	2.3
6, 50–54	63.42	2.9

Table 2. (Continued).

Core-Section (interval in cm)	Sub-bottom depth (m)	>63 μm (%)
Hole 575B (Cont.)		
7, 7–11	64.49	1.3
8-1, 62–66	65.34	1.3
1, 130–134	66.02	1.5
2, 88–92	67.10	1.6
3, 29–33	68.01	3.5
3, 126–130	68.98	2.0
4, 80–84	70.02	2.1
5, 30–34	71.02	2.1
5, 130–134	72.02	2.4
6, 90–94	73.12	1.8
9-1, 30–34	74.12	1.9
1, 135–139	75.17	7.9
2, 91–95	76.23	2.5
3, 33–37	77.15	
9-3, 134–138	78.16	
4, 90–94	79.22	2.9
5, 35–38	80.17	1.8
5, 135–139	81.17	2.8
10-1, 10–17	81.54	2.6
1, 107–114	82.51	5.0
2, 44–51	83.38	11.4
3, 2–9	84.46	4.7
3, 105–112	85.49	5.3
4, 47–54	86.41	3.2
5, 2–9	87.46	2.3
5, 104–111	88.48	2.2
6, 44–51	89.38	3.6
7, 4–11	90.48	4.0
11-1, 46–52	91.39	6.9
2, 3–10	92.47	4.2
2, 106–113	93.50	3.6
3, 43–50	94.37	3.9
4, 3–10	95.47	3.6
4, 104–111	96.48	5.4
5, 47–54	97.41	4.0
6, 2–9	98.46	5.4
6, 92–99	99.36	6.2
12-1, 93–100	100.56	5.8
2, 47–54	101.60	8.9
3, 3–10	102.67	6.7
3, 126–133	103.87	10.0
4, 65–72	104.78	14.0
5, 13–20	105.76	10.2
5, 107–114	106.71	4.4
6, 46–53	107.60	12.4
6, 132–139	108.46	13.7
13-1, 43–50	109.67	5.4
2, 3–10	110.77	7.1
2, 106–113	111.80	9.5
3, 62–69	112.86	5.2
4, 10–17	113.84	4.4
14-1, 92–99	115.06	4.7
2, 45–52	116.09	6.0
3, 5–12	117.18	11.3
3, 91–98	118.05	4.3
4, 12–19	118.76	2.6

Table 3. Oxygen and carbon isotope composition (‰, PDB) of *Globoquadrina venezuelana* (350 to 420 μm) in cores of Holes 573B, 574, 574C, 575A, and 575B.

Core-Section (interval in cm)	Sub-bottom depth (m)	$\delta^{18}O$ (‰)	$\delta^{13}C$ (‰)
Hole 573B			
11-1, 6–10	233.58	0.36	1.85
3, 7–11	236.59	0.62	1.49
12-3, 98–102	247.00	0.83	1.78
4, 146–150	248.98	0.81	1.81
5, 98–102	250.00	0.51	1.94

Table 3. (Continued).

Core-Section (interval in cm)	Sub-bottom depth (m)	$\delta^{18}O$ (‰)	$\delta^{13}C$ (‰)
Hole 573B (Cont.)			
13-2, 28–32	254.30	0.26	1.48
5, 78–80	259.29	0.05	1.36
14-3, 120–124	266.22	0.47	1.19
15-2, 118–122	274.20	0.93	0.98
5, 71–75	278.23	0.95	1.10
16-3, 36–40	284.38	0.92	1.14
17-4, 146–150	296.48	0.71	1.42
5, 82–86	297.34	0.65	1.44
20-1, 119–123	320.21	0.26	0.80
2, 74–78	321.26	0.71	0.50
23-2, 36–40	349.38	1.40	0.52
3, 90–94	351.42	0.70	0.63
Hole 574			
25-1, 11–14	172.63	0.96	1.63
64–69	174.67	0.85	1.80
3, 14–19	175.67	0.92	1.41
26-1, 130–137	178.84	0.20	1.37
3, 130–138	181.84	0.59	1.32
27-2, 123–129	184.96	0.78	1.71
4, 22–29	186.96	0.04	1.89
28-1, 89–97	188.13	0.54	1.75
3, 92–99	191.16	0.87	1.79
4, 42–50	192.16	0.79	1.93
29-2, 50–57	194.24	1.22	1.93
4, 33–40	197.07	−0.26	1.87
30-2, 51–58	199.25	0.52	1.64
3, 2–9	200.26	0.53	1.60
31-1, 2–9	202.26	0.51	1.57
3, 2–8	205.25	0.31	1.69
3, 101–109	206.25	0.11	1.19
Hole 574C			
1-2, 125–129	195.27	0.80	1.59
4, 131–135	200.33	0.12	1.61
2-3, 101–105	208.03	0.67	1.56
5, 101–105	211.03	0.42	1.45
3-2, 15–19	215.17	0.43	1.34
4-1, 34–38	223.36	0.47	1.04
3, 49–53	226.51	0.53	1.21
5-2, 50–54	234.52	0.52	0.77
4, 52–56	237.54	0.45	0.99
6-2, 131–135	244.83	0.89	1.48
3, 82–86	245.84	0.81	1.48
4, 129–133	247.81	0.80	1.28
7-3, 3–7	254.55	0.93	0.72
5, 100–104	258.52	0.81	1.49
8-2, 2–6	262.54	0.80	1.24
3, 51–55	264.53	0.82	1.20
4, 3–7	265.55	0.70	1.38
9-2, 26–30	272.28	0.88	1.13
3, 72–76	274.24	0.98	1.13
10-3, 80–84	283.82	0.27	1.01
5, 74–79	286.76	0.51	1.40
7, 43–47	289.45	0.88	1.25
11-1, 96–100	290.48	1.34	1.19
3, 3–7	292.55	0.39	1.23
12-2, 105–109	301.57	0.56	0.82
3, 146–150	303.48	0.65	1.04
13-1, 94–98	309.46	0.57	1.62
2, 31–35	310.33	0.82	1.37
3, 90–94	312.42	1.43	1.26
14-1, 35–39	318.37	0.50	1.76
2, 78–82	320.30	0.95	1.38
15-2, 37–41	329.39	0.96	1.63
2, 138–142	330.40	0.61	1.20
5, 81–85	334.33	1.01	1.50
16-1, 55–59	337.57	0.73	0.54
18-1, 25–29	356.27	1.19	0.12
20-1, 30–34	375.32	0.84	0.15
4, 2–6	379.54	0.89	0.61
21-2, 80–84	386.82	1.04	0.19
3, 30–34	387.82	1.30	0.44

Table 3. (Continued).

Core-Section (interval in cm)	Sub-bottom depth (m)	$\delta^{18}O$ (‰)	$\delta^{13}C$ (‰)
Hole 575A			
1-1, 2-9	93.85	0.15	2.24
1, 102-109	94.85	0.25	1.75
3, 10-17	96.93	−0.09	1.64
2-4, 32-36	102.04	0.46	1.57
3-2, 53-60	103.17	0.32	1.33
3, 10-19	104.24	0.56	1.59
4-1, 21-29	105.45	0.24	1.35
3, 45-52	108.69	0.52	1.68
5-2, 94-100	111.47	0.69	1.25
4, 2-9	113.56	0.50	1.56
6-1, 61-68	114.74	0.72	1.13
2, 21-28	115.85	0.81	0.93
2, 121-128	116.85	0.40	1.14
7-1, 101-108	119.45	0.84	1.03
2, 142-149	121.36	0.57	0.95
8-1, 53-60	123.67	0.38	1.00
2, 2-9	124.65	0.83	1.08
9-1, 122-129	126.56	0.94	1.31
2, 81-88	127.64	0.78	1.15
10-1, 93-100	128.26	0.72	1.48
3, 2-9	130.35	0.73	1.10
11-2, 102-109	133.15	0.91	1.71
3, 131-138	134.94	0.69	1.35
12-2, 134-141	137.97	0.89	1.32
3, 94-101	139.07	1.01	1.40
13-1, 101-108	139.85	0.88	1.10
3, 6-13	141.89	0.86	1.38
14-1, 111-118	143.05	1.22	1.19
3, 13-20	145.07	1.18	1.28
15-2, 25-31	146.48	0.95	1.24
2, 125-131	147.48	1.06	1.40
16-2, 8-15	149.62	0.85	1.28
3, 54-61	151.58	0.96	1.27
17-2, 53-60	152.07	1.16	1.47
3, 8-15	153.12	0.78	1.24
18-2, 68-75	154.72	1.09	1.36
3, 129-136	156.83	0.93	1.26
19-1, 89-96	157.72	0.74	1.01
3, 2-9	159.85	0.75	1.47
20-1, 22-29	161.06	1.35	1.05
3, 49-56	164.33	1.38	1.05
21-2, 30-37	166.54	1.30	0.90
3, 81-88	168.55	1.21	1.38
22-1, 102-109	169.15	1.08	1.23
2, 133-140	170.97	1.08	1.06
23-1, 92-99	173.06	0.59	1.01
2, 51-58	174.14	0.92	1.10
24-1, 101-109	175.25	0.94	1.42
3, 12-19	177.36	0.70	1.59
25-2, 143-150	180.17	0.71	1.20
3, 103-110	181.27	0.90	1.30
26-1, 132-139	181.46	0.63	1.49
3, 130-137	184.43	1.14	1.74
27-2, 88-97	187.33	1.19	1.43
3, 30-37	188.24	0.52	1.59
28-1, 143-150	188.67	0.64	1.61
3, 14-21	190.38	0.22	1.49
29-1, 141-148	191.15	0.69	1.09
3, 52-59	193.26	0.80	1.67
31-2, 65-72	199.59	0.56	1.48
3, 101-108	201.45	0.78	1.24
32-1, 143-150	202.76	0.83	1.26
3, 48-55	204.81	0.91	0.99
33-2, 50-57	206.34	1.10	0.81
Hole 575B			
2-5, 117-121	19.19	0.69	0.58
6, 107-111	20.59	0.80	0.50
3-2, 45-49	22.97	0.31	0.83
5, 63-67	27.65	0.67	1.07
4-1, 123-127	30.75	0.72	1.13
3, 128-132	33.80	0.58	1.32
5-3, 113-117	43.15	1.30	1.42
4, 144-148	44.96	1.64	1.52
6, 50-54	47.02	1.08	1.44

Table 3. (Continued).

Core-Section (interval in cm)	Sub-bottom depth (m)	$\delta^{18}O$ (‰)	$\delta^{13}C$ (‰)
Hole 575B (Cont.)			
7, 3-7	48.05	1.01	1.18
6-2, 24-28	49.76	1.35	1.60
2, 123-127	50.75	0.87	1.10
3, 69-73	51.71	1.31	1.13
4, 25-29	52.77	0.81	1.27
4, 124-128	53.76	1.25	1.01
5, 85-89	54.87	0.99	1.15
6, 32-36	55.84	0.97	1.37
7-1, 93-97	56.35	1.29	1.37
2, 47-51	57.39	1.42	1.32
3, 3-7	58.45	1.61	1.33
3, 95-99	59.37	0.79	1.28
4, 50-54	60.42	1.20	1.67
5, 3-7	61.45	1.70	1.63
5, 105-109	62.47	1.44	1.42
6, 50-54	63.42	1.37	1.83
8-1, 62-66	65.34	0.98	1.16
1, 130-134	66.02	0.43	1.41
2, 88-92	67.10	1.15	1.34
3, 29-33	68.01	0.91	1.00
3, 126-130	68.98	0.81	1.05
4, 80-84	70.02	1.03	1.10
5, 30-34	71.02	1.22	1.46
5, 130-134	72.02	1.01	1.32
6, 90-94	73.12	0.49	1.17
9-1, 30-34	74.12	1.60	1.67
1, 135-139	75.17	1.20	1.56
3, 33-37	77.15	0.92	1.34
4, 90-94	79.22	1.21	1.48
5, 135-139	81.17	0.80	1.62
10-2, 44-51	83.38	0.90	2.38
5, 2-9	87.46	0.41	1.70
11-3, 43-50	94.37	0.90	1.87
6, 2-9	98.46	0.83	1.81
12-2, 47-54	101.60	0.73	2.32
5, 13-20	105.76	0.73	1.86
13-1, 43-50	109.67	0.86	2.13
2, 106-113	111.80	1.11	1.73
14-2, 45-52	116.09	0.05	1.82
3, 91-98	118.05	−0.09	1.82

from less variable below to high-frequency, high-amplitude variability above, and the benthic foraminifers show a marked increase in $\delta^{18}O$ of about 0.7‰. This increase can be correlated with an abrupt increase in the benthic foraminifer oxygen isotope record of the same amplitude at 155 m at Site 574 (Pisias et al., this volume, and Fig. 5).

Above this sharp ^{18}O enrichment the $\delta^{18}O$ values of *O. umbonatus* continue to increase to values close to 3‰ at a level slightly above level H in the middle Miocene. They retain this high value through the remainder of the section, whereas the ^{18}O values of *G. venezuelana* decrease sharply. The oxygen isotope gradient between *O. umbonatus* and *G. venezuelana* ($\Delta\delta^{18}O_{B-P}$; Table 4) increases progressively from about 1‰ in the F–G interval to about 2‰ in the G–H interval and 2.5‰ at the top of the middle Miocene.

Carbon Isotope Stratigraphy

In the uppermost Oligocene and lowermost Miocene (below level A), the carbon isotope record of *Globoquadrina venezuelana* at Site 574 shows depleted $\delta^{13}C$ values (values less than 1‰). At level A, there is a sharp increase of about 1‰. An interval of enrichment, with mean $\delta^{13}C$ values near 1.5‰, occurs between levels A

Levels	Biostratigraphic and magnetostratigraphic position	Approximate age (Ma)	Chemical signals (decrease ↔ increase)			Position in cores					
						Site 573		Site 574		Site 575	
			$\delta^{18}O$	$\delta^{13}C$	$CaCO_3$	Hole-Core	Depth (m)	Hole-Core	Depth (m)	Hole-Core	Depth (m)
H	Within *Coscinodiscus gigas* var. *diorama* Zone Within upper *Dorcadospyris alata* Zone Within Zone CN5a Within Zone N12	12.5	PF						~112 m (Pisias and Shackleton, this volume)	575B-5	43
G	Within Subzone B of *Cestodiscus peplum* Zone Within lower *Dorcadospyris alata* Zone Witnin Zone CN4 Approximates the N9/N10 boundary	14.6	BF						155 (Pisias and Shackleton, this volume)	upper 575B-9	75
F	Approximates the *Denticulopsis nicobarica/ Cestodiscus peplum* boundary Within the middle of the *Calocycletta costata* Zone Within Zone CN3 Within undifferentiated N6—N8 interval Within magnetic Anomaly 5C	16.5	PF minimum			573B-13	257	574-29/30	197	575A-1 and 575B-14	115
E	Within Subzone A of *Denticulopsis nicobarica* Zone Approximates the *Stichocorys wolffii/Calocycletta costata* boundary Approximates the CN2/CN3 zonal boundary Within undifferentiated N6—N8 interval Within lower reversed interval of magnetic Anomaly 5C	17.5		BF + PF		573B-14	267	574C-3/4	220	575A-6	134 (115 + 19)
D	Approximates the *Craspedodiscus elegans/Triceratium pileus* boundary Within uppermost *Stichocorys delmontensis* Zone Within uppermost Zone CN1c Within Zone N5	18.7						574C-6	244	lower 575A-11	154 (135 + 19)
C	Within lowermost *Craspedodiscus elegans* Zone Within *Stichocorys delmontensis* Zone Within Zone CN1c Within Zone N5	19.5	PF			573B-16 (?)	288	574C-7	257	lower 575A-16	170 (151 + 19)
B	Slightly below the B/C boundary in *Rossiella paleacea* Zone Within lower *Stichocorys delmontensis* Zone Within CN1b Within upper Zone N4	20.7		PF		573B	291	lower 574C-10	287	575-25	199 (180 + 19)
A	Approximates the *Rocella gelida/Rossiella paleacea* boundary Within *Lychnocanoma elongata* Zone Within lower Zone CN1b Within Zone N4	22.7		PF		upper 573B-20	320	574-15/16	335		

Figure 5. Biostratigraphic and magnetostratigraphic position of levels marking changes in the signature of the isotope and carbonate records at DSDP Sites 573, 574, and 575. Ages are derived from the Barron et al. (in press) time scale based on the paleomagnetic time scale of Berggren et al. (in press). BF = benthic foraminifers; PF = planktonic foraminifers.

Table 4. Oxygen and carbon isotope composition (‰, PDB) of the benthic species *Oridorsalis umbonatus* (>250 μm) in cores of Holes 575A and 575B and the difference between $\delta^{18}O$ values of *O. umbonatus* and *G. venezuelana* ($\Delta\delta^{18}O_{B-P}$).

Core-Section (interval in cm)	Sub-bottom depth (m)	$\delta^{18}O$	$\delta^{13}C$	$\Delta\delta^{18}O_{B-P}$
Hole 575B				
2-5, 6-10	18.08	3.13	−2.43	
3-6, 101-105	29.53	2.84	−2.34	
4-3, 128-132	33.80	3.22	−1.35	2.64
6-6, 32-36	55.84	2.98	−0.83	2.01
9-1, 135-139	75.17	2.64	0.05	1.44
10-3, 105-112	85.49	2.10	1.03	
11-3, 43-50	94.37	2.04	0.28	1.14
12-3, 126-133	103.89	2.03	0.31	
Hole 575A				
4-3, 45-52	108.69	2.10	−0.12	1.58
5-4, 2-9	113.56	2.24	−0.61	1.74
6-3, 81-88	117.94	1.68	−0.42	
8-1, 53-60	123.67	2.26	−0.76	1.88
8-1, 102-109	124.15	2.17	−0.12	
12-1, 72-80	135.86	2.13	−0.18	
18-3, 129-136	156.83	2.50	−0.38	1.57
25-3, 103-110	181.27	2.25	−1.13	1.35
31-2, 65-72	199.59	2.56	−0.24	2.00

and B in the lower lower Miocene. These two levels are tentatively identified at Site 573, and level B is placed at Site 575 in the lower part of the sequence. In the next interval, between levels B and E, $\delta^{13}C$ values have slightly decreased averages of about 1.2 to 1.3‰.

Above level E in the upper lower Miocene, there is a marked enrichment in ^{13}C of approximately 1‰ which takes place progressively between levels E and F. This enrichment is directly tied to the reversed interval in lower magnetic Anomaly 5C (lower magnetic Chron 16), which is apparent in cores from Hole 575A and which we have referred to as the Chron 16 Carbon Shift (Vincent et al., 1983). Values of $\delta^{13}C$ remain high (from 1.7‰ to 2.4‰) throughout a large part of the interval between levels F and G, which spans the lower/middle Miocene boundary, then decrease just below level G toward values similar to the preceding lower Miocene values, that is, values averaging 1.2 to 1.3‰. This average characterizes the remainder of the middle Miocene; the values then show a pronounced decrease in the upper Miocene.

Carbonate Stratigraphy

Throughout the uppermost Oligocene and most of the lower Miocene, up to level D, the calcium carbonate records at all three sites display a relatively constant $CaCO_3$ content, with a mean of about 90% and small-amplitude fluctuations. There are no pronounced changes in this interval. However, in the expanded record of Site 574 a slight variation is apparent. The interval of enriched ^{13}C between levels A and B corresponds to an interval of slightly increased carbonate content (Figs. 3 and 5). In this interval the mean $CaCO_3$ content is about 92%, whereas below level A it is about 88%, and above level B up to level D, it is about 90%. The A–B interval of slightly increased $CaCO_3$ percentages is tentatively identified in the condensed record of Site 573 and its upper part at Site 575 (Figs. 2 and 4).

Above level D in the upper lower Miocene, the $CaCO_3$ content decreases markedly, reaching a pronounced minimum of 32 to 65 percent at 114 m, 212 m, and 261 m at Sites 575, 574, and 573, respectively. This pronounced minimum, which occurs between levels E and F in the uppermost lower Miocene, correlates with the Chron 16 Carbon Shift. Above the Chron 16 carbonate minimum, the calcium carbonate content increases again to values of about 90% throughout the remainder of the middle Miocene. However, the fluctuations in this interval are of higher amplitude than in the Oligocene to lower Miocene interval (see site chapters, this volume, for middle Miocene $CaCO_3$ records at Sites 573 and 574).

The uppermost lower Miocene interval of decreased carbonate content is correlated with an interval of reduced preservation of foraminifers (see Figs. 2 to 4). However, the wide sampling interval used for the foraminiferal preservation stratigraphy does not allow a detailed correlation with carbonate stratigraphy.

Near the middle/upper Miocene boundary the carbonate curves at all three sites show a marked change (Fig. 4 and site chapters, this volume). Above this level (throughout the upper Miocene to the Quaternary), there are high-amplitude cyclic fluctuations between high-carbonate and low-carbonate sediments that are paralleled by fluctuations in the abundance of siliceous sediments. This pronounced change in sedimentary regime is widespread in the central equatorial Pacific, where it is seismically traceable (Mayer et al., this volume).

Grain Size Stratigraphy

A detailed analysis of our grain size data is beyond the scope of this chapter. Further, data obtained from paired samples, which are preferable for a statistical analysis of the relationship between sand-sized content and calcium-carbonate content, are unavailable for this study. However, long-term cycles are apparent from a visual examination of the sand-sized content curves in Figures 2 to 4. The cycles are defined by the alternation of (1) intervals of high-amplitude fluctuations with pronounced maxima and higher average values and (2) intervals of low-amplitude fluctuations with smaller average values. An interval of type 1, present at all three sites, occurs just below the boundary between lower Miocene and middle Miocene, immediately above the Chron 16 Carbon Shift and the pronounced decrease in $CaCO_3$ content. Another interval of type 1 at the top of the Site 575 sequence is clearly associated with the high-amplitude carbonate fluctuations.

DISCUSSION

Reading the Record

The stratigraphic signals available refer to the physical state of the ocean and the hydrologic cycle in general, and to the ocean's carbon chemistry, which is affected by life processes and geochemical cycles. Physical conditions are reflected mainly in the $\delta^{18}O$ record, and chemical conditions predominantly in $\delta^{13}C$, carbonate

content, and foraminiferal preservation. Of the various signals, the reasons for the fluctuations in $CaCO_3$ preservation are the simplest to interpret (they are due mainly to saturation of the bottom water), and the reasons for the fluctuations in $\delta^{13}C$ are the most complex. The reasons for grain size fluctuations are also complex. All signals are strongly interdependent, because there is an intimate connection between the physical, chemical, and biological aspects of the system. These matters have been discussed elsewhere (e.g., van Andel et al., 1975; Bender and Keigwin, 1979; Vincent et al., 1980; Berger, 1981; Berger and Vincent, 1981; Vincent and Berger, 1981, in press).

We used the following guidelines in reading the record, which are gleaned, in the main, from the references cited (we do not suggest that our methods are preferable to more detailed analysis):

1. *$\delta^{18}O$* reflects changes in water temperature at the time of growth of the shells, as well as changes in the $^{18}O/^{16}O$ ratio of the surrounding water (which is affected by regional and/or global salinity and the presence or absence of ice caps). The formula of Epstein et al. (1953) applies. The temperature effect is roughly 0.2‰ change in $\delta^{18}O$ per 1°C change in water temperature. To change $\delta^{18}O$ through ice buildup, a change in sea level of between 10 and 20 m (depending on the composition of the ice; see Emiliani, 1955) is necessary to cause a change in $\delta^{18}O$ of about 0.1‰.

2. *$\delta^{13}C$* is regionally influenced by carbon fixation (which increases $\delta^{13}C$) and respiration (which decreases it). The $\delta^{13}C$ value reflects net productivity at the surface and oxygen utilization at depth. Regional patterns are governed by mixing processes in the ocean as well as by chemical processes. Global changes are effected by changes in the overall carbon cycle, notably changes in the ratio of inorganic to organic carbon in source- and sink-terms.

3. *Sand content* is a function of (a) productivity and the relative proportion of large, robust deep-dwelling microfossils, (b) winnowing (which increases sand content) and dilution by fines (which decreases it), and (c) carbonate dissolution (decreases sand content).

4. *Carbonate content* is affected by the rates of supply, dilution, and dissolution of $CaCO_3$. Of these, dissolution is probably the most important in any given interval.

5. *Foraminiferal preservation* is affected by the saturation of bottom waters in carbonate and the supply of organic matter to the seafloor.

The interdependence of these signals is obvious. Hence, we shall adopt the hypothesis that events (peaks or shifts) in different signals that are closely associated in time have a common cause or are part of a causal chain. Because a change in each individual signal can be produced by a number of factors, we need a number of signals to be able to narrow the choices down to the most likely cause. Clearly, the considerable effort that is necessary to establish such multiple-signal stratigraphies can best be justified for continuous records of high resolution, in regions that record events of global significance.

In this respect we are satisfied that the expanded record at Sites 573 to 575 has excellent potential for the paleoceanographic reconstruction of the early to middle Miocene.

A more detailed "multichannel" isotope stratigraphy than could be prepared for this study will be necessary to resolve many paleoceanographic questions. We especially need to complement the isotope record obtained in this study, which was from a deep-living planktonic foraminifer (subsurface water), with a record for the ocean properties at the surface (shallow-dwelling planktonic foraminifers) and at the seafloor (benthic foraminifers).

Correlation between Biostratigraphy and Chemostratigraphy

The levels of change in the isotope and carbonate records summarized in Figure 5 correlate well from site to site through biostratigraphy (Figs. 2 to 4). The age of these levels can thus be estimated with reasonable confidence despite minor discrepancies between the various microfossil zonations at the three sites (Barron et al., this volume).

The sedimentary sequences from Sites 574 and 575 together provide a complete lower Miocene record. The record at Site 573 is incomplete and condensed, and several hiatuses were recognized (see Barron et al. and Theyer et al., both this volume). Because of sediment condensation and the wide sampling interval, the exact position of levels A to H could not be determined at the latter site. Several of these levels are identifiable, however, with even a low-resolution chemostratigraphy when placed in a biostratigraphic framework (Fig. 2).

Other isotope records that are available for comparison with this study are shown in Figure 6 (in back pocket).

Miocene benthic foraminifer isotope records from the equatorial Pacific have been published by Savin et al. (1981) and Woodruff et al. (1981) for DSDP Sites 71, 77, and 289. The first two of these sites are in the same area as the Leg 85 sites (see Fig. 1). The lower and middle Miocene sedimentary sequence at Site 71, to the west of Sites 574 and 575, accumulated at an average rate of approximately 32 m/m.y., which is similar to accumulation rates at the latter two sites (Barron et al., in press). The benthic foraminifer isotope record from Site 71, however, was not obtained from monospecific samples, and it does not encompass more than the lowermost middle Miocene. The section from Site 77, like that from nearby Site 573, is condensed and contains several hiatuses. Site 289, which is on the Ontong Java Plateau in the western equatorial Pacific (latitude: 0°29′S; longitude: 158°30′E; water depth: 2224 m), provides an expanded continuous record of the upper lower Miocene and the entire middle Miocene; the section accumulated at an average rate of approximately 33 m/m.y., varying from 20 m/m.y. to 50 m/m.y. (Andrews et al., 1975; Barron et al., in press). The detailed benthic foraminifer isotope stratigraphy obtained at this site by Savin et al. (1981) and Woodruff et al. (1981) is reproduced in Figure 6.

Vincent et al. (in press) used benthic foraminifers as well as shallow-dwelling and deep-living planktonic foraminifers to establish multiple isotope stratigraphies throughout the Miocene for four DSDP sites in the tropical Indian Ocean. The trends in the isotope stratigraphies for the four sites are similar. Of these four sites we selected Site 216 (on the Ninetyeast Ridge, latitude: 1°27′N; longitude: 90°12′E; water depth: 2247 m) for comparison with the Pacific records (Fig. 6), because the sedimentary sequence at this site, despite its condensation (an average accumulation rate of 5 m/m.y.), provides the most complete and undisturbed record for the early and middle Miocene (Vincent et al., in press). It is also the only site that yielded siliceous biostratigraphic control throughout the interval.

We have made no attempt here to present data plotted against time, because as of this writing discrepancies between the time scales used by various authors have not been resolved. The middle Miocene time scale has been revised since the start of this study (see the differences between the time scales used in the site chapters and in Barron et al., this volume), and we felt it inappropriate to attempt to work out detailed correlations between various records at this time.

Berggren et al. (in press) have recently proposed the correlation of Anomaly 5 with Chron 11 (as originally proposed by Foster and Opdyke, 1970), instead of correlating Anomaly 5 with Chron 9, the correlation many authors have utilized in constructing time scales during the last 10 yr. Berggren's proposed revision results in age estimates approximately 1.5 to 2 m.y. younger for biostratigraphic datum levels in the interval between approximately 6.5 and 13.8 Ma. It also implies considerable changes in previously published sedimentation rate profiles.

Despite the varying sampling density and varying biostratigraphic resolution of the various records shown in Figures 2 to 4 and Figure 6, a number of the chemostratigraphic markers A to H can be identified in all records. These thus provide signals of the utmost importance for chronostratigraphic correlation. Careful stacking of chemostratigraphic signals from different records will greatly enhance the precision of correlation between different ocean basins and will provide a precious tool for global paleoceanographic reconstruction. Once a chemostratigraphic signal is shown to be global, it becomes a superior time marker, and one to which biostratigraphy must defer. An example of discrepancies in the biostratigraphic position of a global chemostratigraphic marker, seen in Figure 6, is discussed below.

Level G marks an abrupt step in the benthic foraminifer $\delta^{18}O$ record toward higher values. The step occurs within the mid-Miocene oxygen enrichment. This level corresponds to the N9/N10 foraminiferal zonal boundary identified by Saito (this volume) at both Sites 575 and 574 (see Figs. 5 and 6). From an examination of Figure 6, however, it appears that level G has a higher stratigraphic position with respect to the foraminiferal zonation at Site 289 and a lower one at Site 216. At Site 289 level G, at approximately 450 m, falls in Core 48, in the upper part of Zone N10 identified by Srinivasan and Kennett (1981a, b), whereas at Site 216 it lies in the uppermost part of an undifferentiated N8–N9 interval as given by Berggren et al. (1974) (Fig. 6).

The precise placement of foraminiferal zonal boundaries is often made difficult by taxonomic ambiguities and/or the rarity of zonal nominate taxa. Zonal boundaries defined by the FAD (first appearance datum) of a species are placed by many biostratigraphers at the level of first appearance of a morphotype of this species, which is older than the level of "evolutionary appearance" of that species. The latter has been defined as "the level at which more than half of the individuals in the population have the character(s) that distinguishes the species from its ancestor or descendant" (Riedel and Sanfilippo, 1971, p. 1530). Different interpretations of foraminiferal data by various workers in identifying levels of first appearance may be responsible for discrepancies in zonal assignments.

The N9/N10 boundary is defined by the FAD of *Globorotalia peripheroacuta* (Blow, 1969; Srinivasan and Kennett, 1981a, b). Saito (this volume) places the N9/N10 boundary at the first morphotypic appearance of *G. peripheroacuta* at approximately 155 m at Site 574 (between Sections 2 and 3 of Core 574-21) and approximately 74 m at Site 575 (between Sections 1 and 2 of Core 575-9), that is, at a level that nearly coincides with the depth of level G at both sites. Srinivasan and Kennett (1981a, b) may have given the N9/N10 boundary at Site 289 a lower stratigraphic position with respect to level G because their interpretation of the FAD of *G. peripheroacuta* was different from Saito's. Srinivasan and Kennett report "the first evolutionary appearance" of this species at Site 289 in Core 49 (Srinivasan and Kennett, 1981a, p. 425), and their generalized range chart (Srinivasan and Kennett, 1981b, p. 502) shows the bottom of continuous occurrence of *G. peripheroacuta* in Core 49. However, no detailed chart of species occurrences has been published by these authors.

Although the N9/N10 boundary at Site 216, as drawn on Figure 6, has a stratigraphic position relative to level G higher than at Sites 574 and 575, foraminiferal data from this site support the correlation of level G with the N9/N10 boundary. This boundary is placed on Figure 6 in the middle of Core 216A-5, as originally drawn by Berggren et al. (1974) and followed by Vincent (1977), at the base of the common occurrence of *G. peripheroacuta*. Rare specimens referable to this species, however, are reported on Berggren et al.'s (1974) range charts below that stratigraphic horizon, ranging down to lower Core 5A near level G.

At all sites examined here, level G falls within the calcareous nannofossil Zone CN4 and the *Dorcadospyris alata* radiolarian Zone. At both Sites 574 and 575, level G is slightly below the *Cestodiscus peplum/C. lewisianus* diatom zonal boundary (Barron, this volume). This boundary is marked by the LAD of *C. peplum*, which has been paleomagnetically dated within magnetic Chron 15 (Burckle, 1978) and occurs at approximately 14.1 Ma according to the Barron et al. (in press) time scale used in this study. There is no biostratigraphic control from diatom data at either Site 289 or 216. The siliceous rec-

ord at Site 289 is very poor and barren of diagnostic diatoms (Barron, pers. comm., 1983), and diatom data from Site 216 are not yet available.

The importance of obtaining biostratigraphic and chemostratigraphic data from paired samples for the precise timing of chemostratigraphic signals should be emphasized. Hole-to-hole correlations at a single site that are based solely on sub-bottom depth often require offsets because of the uncertainty of the mudline position. Such offsets had to be made between several Leg 85 holes (see, for example, the 19-m offset between Holes 575A and 575B, as explained in the Fig. 4 caption). The isotope stratigraphies presented in this study (Figs. 2 to 4) are plotted against a composite biostratigraphic column (one established from the various holes at each site; Barron et al., this volume); the holes used in establishing the composite are not always the same as those used in our own analyses. Discrepancies in the correlation of the stratigraphies at the various sites should be resolved when higher resolution biostratigraphic and chemostratigraphic studies can be conducted from paired samples.

PALEOCEANOGRAPHIC IMPLICATIONS OF EARLY MIOCENE EVENTS

The data presented in Figures 2 to 4 and 6 clearly show the succession of events preceding the middle Miocene ^{18}O enrichment and allow the timing of these events to be established.

During the warming trend that characterized the second half of the early Miocene (between approximately 19.5 and 16.5 Ma, or between levels C and F), the following succession of events took place. Fluctuations in $\delta^{18}O$ values are subdued, and the $\delta^{13}C$ record is uneventful. At the same time, sand content decreases (C to D); then $CaCO_3$ preservation and carbonate content decrease (D to E). We suggest that warming (as revealed by the $\delta^{18}O$ signal) is associated with declining bottom current activity (as evidenced by winnowing, which is reflected in the sand content), and that a sea level rise associated with warming (D to E) tends to remove carbonate to the shelves, increasing dissolution on the deep-sea floor (shelf–basin fractionation, which is indicated by $CaCO_3$ content and foraminiferal preservation).

After these events, there is a sharp increase in carbonate dissolution near level E that coincides with the onset of the Chron 16 Carbon Shift, where $\delta^{13}C$ values become higher. The presence of a shift in both the planktonic and benthic foraminifer records suggests that a change in the composition of the ocean is involved, that is, a change in the entire geochemical cycle. We propose that the production of organic carbon increases at this point, at the expense of carbonate. The underlying mechanism might be increased upwelling due to thermocline development (which is evidenced by the first appearance of *Sphaeroidinellopsis* and other planktonic forms with heavy cortices in the tropics at this time). The increased deposition of organic carbon on widely flooded shelves with the shelf edge intersecting the oxygen minimum might also be appealed to. Both thermocline development and equatorial upwelling may be reflected in the increasing sand content, which may result from an increase in heavy, deep-dwelling species. Increased bottom current activity also may contribute to this trend.

The Chron 16 Carbon Shift marks the levels E and F. It lasts about 1 m.y., beginning approximately at 17.5 Ma. After the carbon shift ends, the middle Miocene cooling begins, a sequence that suggests the above-mentioned geochemical preconditioning of the ocean–atmosphere system for entry into a modern, glacier-dominated world.

The pattern of cooling is not easily decipherable from the $\delta^{18}O$ records. A cooling step is clearly indicated immediately after the 16.5 Ma level (just above level F) in both the benthic foraminifer records (see Sites 216 and 289 in Fig. 6) and the planktonic foraminifer records (see Sites 216 and 575 in Fig. 6), but it is short, and warming recurs between 16.5 and 14.6 Ma (between levels F and G). Within the F–G interval, there is a pronounced excursion toward lower $\delta^{18}O$ values in the *Globoquadrina venezuelana* isotope record from the tropical Indian Ocean (DSDP Sites 216 and 238; Fig. 6). During the period immediately following F (end of carbon shift, first cooling pulse), the system seems to have been unstable, as recorded in large fluctuations in sand content and carbonate content. A relaxation toward pre-E conditions is then indicated in all signals except $\delta^{13}C$, which remains unusually positive.

At 14.6 Ma (level G), a sharp step in ^{18}O enrichment in benthic foraminifers coincides with the change in regime in the *G. venezuelana* $\delta^{18}O$ record at Site 575. The increase in instability shown by the planktonic foraminifer record (high-amplitude, high-frequency fluctuations) above this level may be an effect of ice buildup at this time. However, this change in regime is not apparent in the *G. venezuelana* record from the Indian Ocean.

An increase in $\delta^{18}O$ of 1‰ or more is clear in all benthic foraminifer records between 14.6 and 12.5 Ma (from levels G to H). There is also an overall increase in $\delta^{18}O$ values in the planktonic foraminifer isotope records in this interval, but it is of much smaller amplitude. Whereas above level H the $\delta^{18}O$ benthic foraminifer values remain high, the $\delta^{18}O$ planktonic foraminifer values decrease. Thus, if ice buildup caused the ^{18}O enrichment it must have been counteracted by the warming of tropical surface waters. In the absence of such counteraction no more than about one-third of the 1‰ $\delta^{18}O$ increase can be attributed to an ice buildup. Therefore, the evidence for a large ice buildup (one causing more than 20 m of sea level change) is not convincing at this time.

The $\delta^{18}O$ records through the middle and late Miocene are characterized by the increasing separation of benthic and planktonic foraminifer $\delta^{18}O$ values. The separation reflects an increase in the planetary temperature gradient during that time interval, and the increased temperature gradient resulted in a more stably stratified ocean, presumably one with a stronger thermocline and hence increased equatorial and coastal upwelling. We have discussed these trends before (Berger et al., 1981; Vincent and Berger, 1981; Vincent et al., in press).

After the Chron 16 Carbon Shift the $\delta^{13}C$ values of both the benthic and planktonic foraminifers remain high during most of the interval between levels F and G and

then relax progressively to early Miocene values. This broad lower to middle Miocene carbon maximum, which we call the "Monterey Carbon Excursion" (Vincent and Berger, in press), appears to be correlated with the deposition of organic-carbon-rich sediments around the margin of the North Pacific in the Monterey Formation of California and its equivalents. We have elaborated elsewhere on the significance of this correlation (Vincent and Berger, in press). The organic-carbon-rich Monterey rocks and equivalents are the result of coastal upwelling, which arose because of the development of a permanent strong thermocline. The sediments in the upwelling areas were deposited, in part, under anaerobic conditions, which led to the excess extraction of organic carbon from the ocean. A decrease in the rate of carbon extraction (due to the exhaustion of nutrient phosphorus) would have allowed relaxation toward initial values. Alternatively, or concurrently, a drop in sea level due to ice buildup would have led to the increased erosion of shallow areas, with the preferential erosion of organic matter. This process could have helped shift the $\delta^{13}C$ signal back toward negative values. From a simple geochemical balance model, Vincent and Berger (in press) estimated the amount of excess organic carbon extracted during the course of the Monterey event to be between 40 and 80 atmospheric carbon masses. This amount corresponds to that present in the ocean, that is, one ocean carbon mass.

It is remarkable that a major carbonate dissolution event is associated with the heavy carbon excursion. The same situation occurs at two other equatorial Pacific DSDP sites (71 and 289), where a pronounced carbonate minimum ("16 g" of Dunn, 1982) occurs in the same relative position with respect to the carbon shift shown by Savin et al. (1981) and Woodruff et al. (1981). It corresponds to a prominent traceable acoustic horizon throughout the equatorial Pacific, the "Lavender" reflector of Mayer et al. (this volume). The maximum dissolution is coeval with the Chron 16 Carbon Shift (see the pronounced carbonate minima between levels E and F in Figs. 2 to 4; at Site 289 the pronounced carbonate minimum identified by Dunn, pers. comm., 1983, occurs between levels E and F, as marked in Fig. 6). The dissolution increase, however, appears to precede the ^{13}C enrichment, as evidenced by the inflection point on the carbon curves at level D. The diatom biostratigraphy for Site 573 suggests that there is a hiatus at this time (Barron, this volume). This short hiatus, which corresponds to NH1b of Barron and Keller (1982), has been observed in a number of deep-sea sequences in other parts of the Pacific.

A decrease in carbonate deposition tied to an increase in ^{13}C is opposite to what one would expect from Broecker's (1982) model, in which increased $\delta^{13}C$ is tied with increased $CaCO_3$ deposition. We used an argument similar to Broecker's when we discussed the association of the late Miocene Chron 6 Carbon Shift toward light $\delta^{13}C$ values with a carbonate dissolution event (Vincent et al., 1980).

The relationship between $CaCO_3$ content and ^{13}C signals is obviously far from simple. The complexity of the interactions is illustrated in this study by the occurrence of high ^{13}C with either dissolution (as in the Chron 16 Carbon Shift interval E–F) or increased $CaCO_3$ (as in the earlier A–B interval) (Figs. 3 and 5). Different mechanisms must be involved. In principle, it seems safe to say that a change in the state of the system, in whatever direction, should lead to the redistribution of carbonate and other chemically active sediments. Thus, hiatus formation must occur in some places whenever there is change, as long as the change is large enough and the sediment is mostly carbonate. If this is correct, any strong global shift of $\delta^{18}O$ and/or $\delta^{13}C$, in either direction, becomes a candidate for hiatus formation.

CONCLUSIONS

Because causes precede effects, it is important for an understanding of the mechanisms involved in the evolution of ocean conditions to identify with precise timing the sequential order of events. In this respect, the sedimentary sequences studied here are the best acquired to date for high-resolution paleoceanographic reconstruction during the period of preconditioning before the major middle Miocene cooling.

It is premature to attempt to identify causes for all paleoceanographic changes. Our explanations should be considered hypotheses only. The development of additional detailed multichannel stratigraphies (chemostratigraphies combined with biostratigraphy and changes in faunal and floral composition), which permit the separation of the numerous variables involved in changes in environmental conditions, will allow a better understanding of the mechanisms involved in changes in the ocean–atmosphere system.

ACKNOWLEDGMENTS

We are very grateful to Wolf Berger for many stimulating discussions and for reviewing our manuscript. Our work is supported by NSF Grants OCE83-10518 and OCE83-14984.

REFERENCES

Andrews, J. E., Packham, G., et al., 1975. *Init. Repts. DSDP*, 30: Washington (U.S. Govt. Printing Office).

Barron, J. A., and Keller, G., 1982. Widespread Miocene deep-sea hiatuses: coincidence with periods of global cooling. *Geology*, 10: 577–581.

Barron, J. A., Keller, G., and Dunn, D. A., in press. A multiple microfossil biochronology for the Miocene. *In* Kennett, J. P. (Ed.), *The Miocene Ocean: Paleoceanography and Biogeography.* Mem. Geol. Soc. Am. 163.

Bender, M. L., and Keigwin, L. D., Jr., 1979. Speculations about the upper Miocene change in abyssal Pacific dissolved bicarbonate $\delta^{13}C$. *Earth Planet. Sci. Lett.*, 45:383–393.

Berger, W. H., 1981. Paleoceanography: the deep-sea record. *In* Emiliani, C. (Ed.), *The Oceanic Lithosphere: The Sea* (Vol. 7): New York (Wiley-Interscience), 1437–1519.

_____, 1982. Deep-sea stratigraphy: Cenozoic climate steps and the search for chemo-climatic feedback. *In* Einsele, G., and Seilacher, A. (Eds.), *Cyclic and Event Stratification:* Berlin (Springer Verlag), 121–157.

Berger, W. H., and Killingley, J. S., 1977. Glacial Holocene transition in deep-sea carbonates: selective dissolution and the stable isotope signal. *Science*, 197:563–566.

Berger, W. H., Killingley, J. S., and Vincent, E., 1978. Stable isotopes in deep-sea carbonates: Box Core ERDC-92, west equatorial Pacific. *Oceanologica Acta*, 1:203–216.

Berger, W. H., and Vincent, E., 1981. Chemostratigraphy and biostratigraphic correlation: exercises in systematic stratigraphy. *Proc.*

26th Internat. Geol. Congress, Geology of Oceans Symposium (Paris, 1980). Spec. Publ. Oceanologica Acta, 115–127.

Berger, W. H., Vincent, E., and Thierstein, H. R., 1981. The deep-sea record: major steps in Cenozoic ocean evolution. *Spec. Publ. Soc. Econ. Paleontol. Mineral.*, 32:489–504.

Berger, W. H., and von Rad, U., 1972. Cretaceous and Cenozoic sediments from the Atlantic Ocean. *In* Hayes, D. E., Pimm, A. C., et al., *Init. Repts. DSDP*, 14: Washington (U.S. Govt. Printing Office), 787–954.

Berger, W. H., and Winterer, E. L., 1974. Plate stratigraphy and the fluctuating carbonate line. *In* Hsü, K. J., and Jenkyns, H. (Eds.), *Pelagic Sediments on Land and Under the Sea.* Spec. Publ. Internat. Assoc. Sedimentol., 11–48.

Berggren, W. A., Kent, D. V., and Van Couvering, J. A., in press. Neogene geochronology and chronostratigraphy. *In* Snelling, N. J. (Ed.), *Geochronology and the Geological Records.* Spec. Pap. Geol. Soc. London.

Berggren, W. A., Lohmann, G. P., and Poore, R. Z., 1974. Shore laboratory report on Cenozoic planktonic foraminifera: Leg 22. *In* von der Borch, C. C., Sclater, J. G., et al., *Init. Repts. DSDP*, 22: Washington (U.S. Govt. Printing Office), 635–655.

Berggren, W. A., and Schnitker, D., 1983. Cenozoic marine environments in the North Atlantic and Norwegian–Greenland Sea. *In* Bott, M. H. P., Saxon, S., Talwani, M., and Thiede, J. (Eds.), *Structure and Development of the Greenland–Scotland Ridge:* Plenum, 495–548.

Blanc, P. L., Rabussier, D., Vergnaud Grazzini, C., and Duplessy, J. C., 1980. North Atlantic deep water formed by the later middle Miocene. *Nature*, 289:553–555.

Blow, W. H., 1969. Late middle Eocene to Recent planktonic foraminiferal biostratigraphy. *In* Brönniman, P., and Renz, H. H. (Eds.), *Proc. First Internat. Conf. Planktonic Microfossils* (Geneva, 1967): Leiden (Brill), 199–421.

Broecker, W. S., 1982. Glacial to interglacial changes in ocean chemistry. *Prog. Oceanogr.*, 11:151–197.

Bukry, D., 1975. Phytoplankton stratigraphy, southwest Pacific, Deep Sea Drilling Project, Leg 30. *In* Andrews, J. E., Packham, G., et al., *Init. Repts. DSDP*, 30: Washington (U.S. Govt. Printing Office), 539–547.

Burckle, L. H., 1978. Early Miocene to Pliocene diatom datum levels for the equatorial Pacific. *Proc. Second Working Group Mtg., Biostratigr. Datum-Planes Pacific Neogene, IGCP Project 114* (Bandung, Indonesia, May 30–June 1, 1977). Spec. Publ. Geol. Res. Dev. Ctr., 1:25–44.

Dunn, D. A., 1982. Miocene sediments of the equatorial Pacific Ocean: carbonate stratigraphy and dissolution history [Ph.D. dissert.]. Univ. Rhode Island, Narragansett.

Emiliani, C., 1955. Pleistocene temperatures. *J. Geol.*, 63:538–578.

Epstein, S., Buchsbaum, R., Lowenstam, H. A., and Urey, H. C., 1953. Revised carbonate-water isotopic temperature scale. *Geol. Soc. Am. Bull.*, 64:1315–1326.

Foster, J. H., and Opdyke, N. D., 1970. Upper Miocene to Recent magnetic stratigraphy in deep-sea sediments. *J. Geophys. Res.*, 75: 4465–4473.

Holdsworth, B. K., 1975. Cenozoic Radiolaria biostratigraphy: Leg 30: tropical and equatorial Pacific. *In* Andrews, J. E., Packham, G., et al., *Init. Repts. DSDP*, 30: Washington (U.S. Govt. Printing Office), 499–537.

Johnson, D. A., 1974. Radiolaria from the eastern Indian Ocean, DSDP Leg 22. *In* von der Borch, C. C., Sclater, J. G., et al., *Init. Repts. DSDP*, 22: Washington (U.S. Govt. Printing Office), 521–575.

Keigwin, L. D., and Keller, G., 1984. Middle Oligocene climatic change from equatorial Pacific DSDP Site 77. *Geology*, 12:16–19.

Lancelot, Y., 1978. Relations entre évolution sédimentaire et tectonique de la Plaque Pacifique depuis le Crétacé Inférieur. *Mem. Soc. Geol. Fr. 134.*

Matthews, R. K., and Poore, R. Z., 1980. Tertiary $\delta^{18}O$ record and glacio-eustatic sea-level fluctuations. *Geology*, 8:501–504.

Riedel, W. R., and Sanfilippo, A., 1971. Cenozoic Radiolaria from the western tropical Pacific, Leg 7. *In* Winterer, E. L., et al., *Init. Repts. DSDP*, 7: Washington (U.S. Govt. Printing Office), 1529–1672.

Savin, S. M., Douglas, R. G., Keller, G., Killingley, J. S., Shaughnessy, L., Sommer, M. A., Vincent, E., and Woodruff, F., 1981. Miocene benthic foraminiferal isotope records: a synthesis. *Mar. Micropaleontol.*, 6:423–450.

Savin, S. M., Douglas, R. G., and Stehli, F. G., 1975. Tertiary marine paleotemperatures. *Geol. Soc. Am. Bull.*, 86:1499–1510.

Schnitker, D., 1980a. North Atlantic oceanography as possible cause of Antarctic glaciation and eutrophication. *Nature*, 284:615–616.

_____, 1980b. Global paleoceanography and its deep water linkage to the Antarctic glaciation. *Earth Sci. Rev.*, 16:1–20.

Shackleton, N. J., and Kennett, J. P., 1975. Paleotemperature history of the Cenozoic and the initiation of Antarctic glaciation: oxygen and carbon isotope analyses in DSDP Sites 277, 279 and 281. *In* Kennett, J. P., Houtz, R. E., et al., *Init. Repts. DSDP*, 29: Washington (U.S. Govt. Printing Office), 743–756.

Srinivasan, M. S., and Kennett, J. P., 1981a. A review of Neogene planktonic foraminiferal biostratigraphy: applications in the equatorial and South Pacific. *In* Warme, J. E., Douglas, R. G., and Winterer, E. L. (Eds.), *The Deep Sea Drilling Project: A Decade of Progress.* Spec. Publ. Soc. Econ. Paleontol. Mineral., 32:395–432.

_____, 1981b. Neogene planktonic foraminiferal biostratigraphy and evolution: equatorial to subantarctic South Pacific. *Mar. Micropaleontol.*, 6:499–533.

van Andel, T. H., Heath, G. R., and Moore, T. C., Jr., 1975. Cenozoic history and paleoceanography of the central equatorial Pacific. *Mem. Geol. Soc. Am. 143.*

Vincent, E., 1977. Indian Ocean Neogene planktonic foraminiferal biostratigraphy and its paleoceanographic implications. *In* Heirtzler, J. R., Bolli, H. M., Davies, T. A., Saunders, J. B., et al. (Eds.), *Indian Ocean Geology and Biostratigraphy:* Washington, D.C. (Am. Geophys. Un.), 469–584.

Vincent, E., and Berger, W. H., 1981. Planktonic foraminifera and their use in paleoceanography. *In* Emiliani, C. (Ed.), *The Oceanic Lithosphere: The Sea* (Vol. 7): New York (Wiley Interscience), 1025–1119.

_____, 1984. Carbon dioxide and Antarctic ice-buildup in the Miocene: the Monterey hypothesis. *Chapman Conf. on Natural Variations in Carbon Dioxide and the Carbon Cycle* (Tarpon Springs, Florida, Jan. 9–13, 1984). (Abstract)

_____, in press. Carbon dioxide and polar cooling in the Miocene: the Monterey hypothesis. *In* Sundquist, E. T., and Broecker, W. S. (Eds.), *The Carbon Cycle and Atmospheric CO_2: Natural Variations Archaean to Present.* Monogr. Ser. Am. Geophys. Union 32.

Vincent, E., Killingley, J. S., and Berger, W. H., 1980. The magnetic epoch-6 carbon shift: a change in the ocean's $^{13}C/^{12}C$ ratio 6.2 million years ago. *Mar. Micropaleontol.*, 5:185–203.

_____, 1983. The Chron-16 Carbon Event in the Miocene Indian Ocean. *Geol. Soc. Am. Abstr. Progr.*, 15:712. (Abstract)

_____, in press. Miocene oxygen and carbon isotope stratigraphy of the tropical Indian Ocean. *In* Kennett, J. (Ed.), *The Miocene Ocean: Paleoceanography and Biogeography.* Mem. Geol. Soc. Am. 163.

Winterer, E. L., 1973. Sedimentary facies and plate tectonics of equatorial Pacific. *Am. Assoc. Pet. Geol. Bull.*, 57:265–282.

Woodruff, F., Savin, S. M., and Douglas, R. G., 1981. Miocene stable isotope record: a detailed deep Pacific Ocean study and its paleoclimatic implications. *Science*, 212:665–668.

Date of Initial Receipt: 30 January 1984
Date of Acceptance: 6 March 1985